THESIS FOR THE DEGREE OF LICENTIATE OF ENGINEERING

Alkali Metal Stripping and Plating in Liquid Electrolytes

JOSEF RIZELL

Department of Physics

CHALMERS UNIVERSITY OF TECHNOLOGY

Gothenburg, Sweden 2022

Alkali Metal Stripping and Plating in Liquid Electrolytes
JOSEF RIZELL

Department of Physics
Chalmers University of Technology
SE-412 96 Gothenburg
Sweden
Telephone + 46 (0)31-772 1000

Printed by Chalmers Reproservice
Gothenburg, Sweden 2022

Alkali metal stripping and plating in liquid electrolytes

Josef Rizell
Department of Physics
Chalmers University of Technology

Abstract

Batteries have relatively modest energy densities compared to fossil fuels. In the efforts to make battery-driven transport solutions and technologies competitive with gasoline-powered alternatives, it is important to develop batteries with higher energy densities. This can be enabled by utilizing different electrode materials than what is currently done. For instance, lithium metal is one of the electrode materials which can enable the highest theoretical energy densities. Similarly, using metal anodes can pave way for more sustainable materials solutions based on e.g. sodium, potassium or magnesium. During charging in batteries with a metal anode, ions from the electrolyte are plated on the electrode, and during discharge, the metal is stripped from the electrode. These processes are associated with several problems hindering the practical application of metal anodes. For instance, dendritic or uneven growth can cause short circuits and lead to loss of active material. Further, side reactions can consume both electrolyte and active material. A fundamental understanding of the stripping and plating process is needed to solve these problems. In this thesis, electrochemical measurements are used to understand the fundamental steps of the alkali metal plating and stripping process using Li and K metal electrodes. Additionally, the impact of the electrolyte composition, particularly the salt concentration, on alkali metal anodes is investigated. Cycling performance is evaluated and interphase formation is probed with *in situ* neutron reflectometry.

Keywords: Metal anodes, Potassium, Lithium, Stripping, Plating, Nucleation, Highly Concentrated Electrolytes

List of Papers

This thesis is based on the work contained in the following papers:

I High-Energy and Long-Lifespan Potassium–Sulfur Batteries Enabled by Concentrated Electrolyte.
Suyeong Lee, Hyeona Park, Josef Rizell, Un-Hyuck Kim, Yangyang Liu, Xieyu Xu, Shizhao Xiong, Aleksandar Matic, Adi Tiara Zikri, Hyokyeong Kang, Yang-Kook Sun,* Jaekook Kim,* and Jang-Yeon Hwang*
Adv. Funct. Mater. 2022, 2209145.

II Neutron Reflectometry study of SEI formation in highly concentrated electrolytes.
Josef Rizell, Anton Zubayer, Matthew Sadd, Filippa Lundin, Nataliia Mozhzhukhina, Grzegorz Greczynski, Jens Birch, Alexei Vorobiev, Shizhao Xiong and Aleksandar Matic
Manuscript.

III Electrochemical signatures of potassium plating and stripping.
Josef Rizell, Wojciech Chrobak, Nataliia Mozhzhukhina, Shizhao Xiong and Aleksandar Matic
Manuscript.

Contribution Report

I JR performed Raman spectroscopy measurements and analyzed the data, performed density & viscosity measurements, wrote corresponding parts of the manuscript and participated in the revision of the full manuscript.

II SX and AM proposed the reflectivity experiment. JR planned the experiment and designed the cell with input from MS, AZ, FL, NM, AV, SX and AM. AZ performed the sputtering with the support of JR, GG and JB. JR performed the electrochemical measurements, XPS measurements and wrote the manuscript. SX, AM and JR revised the manuscript.

III JR planned the experiments with NM, SX and AM. JR performed and analyzed all experiments, with the support of WC. JR wrote the manuscript and revised it together with AM, SX and NM.

Table of Contents

Chapter 1 - Introduction

For the past centuries, fossil fuels have not only been one of the most important energy sources for our society, but also one of the most important energy storage solutions. Fossil fuels store energy in chemical form, which can be converted into useful work in a combustion engine. As fossil fuels are replaced with renewable energy sources to reduce greenhouse gas emissions, also new ways to store the energy are required.

Batteries can be used to store the energy from renewable energy production but suffer from a much lower energy density than fossil fuels. The energy density of gasoline, 12 000 Wh/kg,[1] is almost two orders of magnitude higher than state-of-the-art (lithium-ion) batteries, 260 Wh/kg (on cell level)[2]. This difference in energy density is a major drawback for technological applications powered by electricity compared to fossil fuels. For instance, around 25% of the weight of a battery electric vehicle is made up of the battery, whereas the fuel makes up only around 3% of the weight in a gasoline car.[1] It is evident that the gravimetric energy density of the battery can pose a serious hurdle in replacing fossil fuels with renewables. This thesis will focus on electrode materials that can help improve the energy density of batteries.

Due to its high specific capacity and low reduction potential, lithium (Li) metal is one of the most interesting electrode materials for high energy density batteries. During discharge in a lithium metal battery, Li-ions are stripped from the metal electrode and when the battery is charged, they are plated back onto the electrode (see figure 1.1). Despite the high energy densities theoretically attainable with this type of electrode, the practical application of rechargeable Li metal batteries has so far been hindered by the tendency for Li to be deposited unevenly on the electrode.[3] The uneven Li deposits can short-circuit the cell, causing failure and potential safety issues, or lead to loss of active material which limits the cycle life of the battery. These problems need to be addressed before Li metal electrodes can be viable to use in commercial rechargeable batteries.

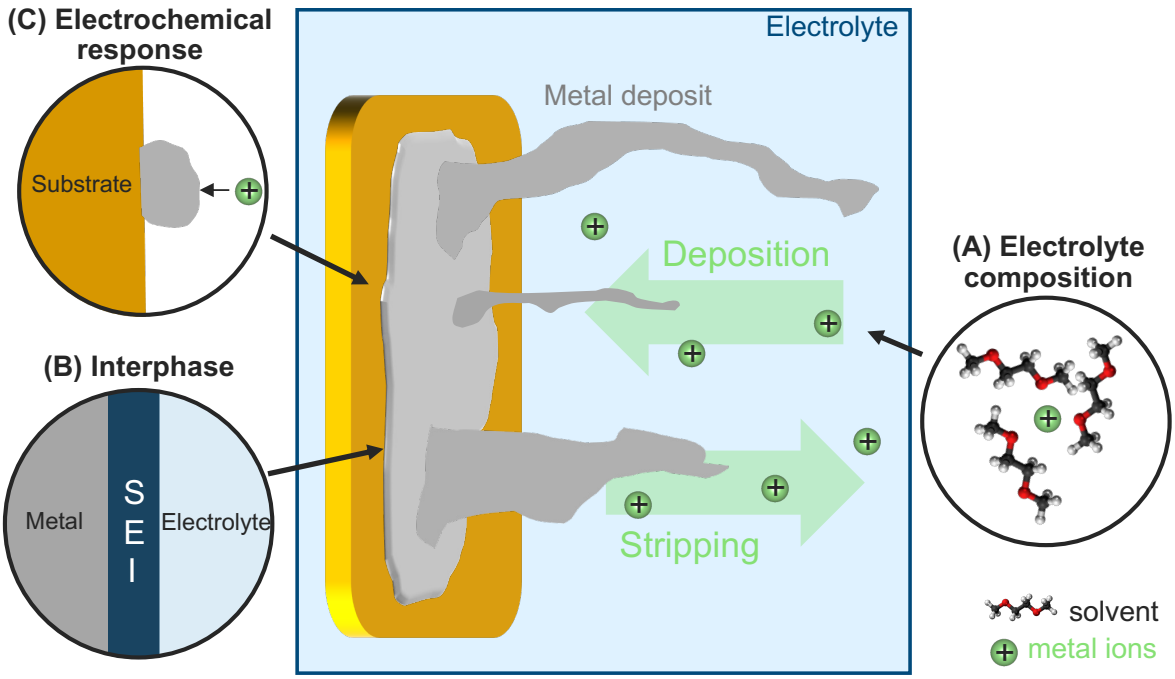

Figure 1.1. Schematic of alkali metal deposition and stripping in liquid electrolytes, highlighting the aspects studied in this thesis.

Due to the scarcity of Li resources, batteries based on other elements have also been heavily researched. The alkali metals sodium (Na) and potassium (K), have abundances of 2.3%[4] and 1.5%[5] in the earth's crust, several orders of magnitude more than Li (0.0017%[4]). These metals can also be used as electrode materials and store energy via reactions analogous to those happening at lithium metal electrodes.[6,7] However, the higher weights of the Na and K atoms compared to Li, make Na- and K-metal batteries unable to match the energy densities of Li metal batteries. Still, Na and K metal are the highest energy electrode (anode) materials than can be conceived for batteries based on Na^+ or K^+ transport. Further, studying these chemically more reactive alkali metal electrodes could bring light to general properties of alkali metal electrodes, which were not previously discerned when Li-metal was studied.

Several strategies aiming to solve the problems faced by alkali metal electrodes focus on the electrolyte composition. In its simplest form, an electrolyte for alkali metal anodes contains a salt, where the cationic species is an alkali ion, and a solvent. Changing the salt and solvent combinations or adding different additives, has been observed to greatly impact both cell performance and electrode morphologies.[8,9] Moreover, the salt concentration in the electrolyte can also alter the cell performance, in particular, electrolytes with high salt concentrations have been shown to suppress dendrite formation and allow stable cycling for many cycles.[10,11] Yet, the mechanism for this improvement is not fully understood. In this thesis, one of the aims is to investigate how electrolyte salt concentration affects the cycling and properties of alkali metal anodes.

The electrolyte composition will also affect the properties of the surface film, known in the battery community as the solid electrolyte interphase (SEI), which forms on alkali metal

electrodes. Due to their high reactivity, alkali metal electrodes will spontaneously react with the electrolyte, covering them in a thin surface film made from electrolyte decomposition products.[12,13] This film is often attributed a deciding role in which type of morphology the metal deposits exhibit and how reversible the stripping/plating process is.[14] In this work, the solid electrolyte interphases in electrolytes with different salt concentrations have been studied using *in situ* neutron reflectometry measurements.

Finally, besides electrolytes with high salt concentrations, numerous different strategies have been attempted to solve the problems associated with alkali metal stripping and plating. For instance, a wide range of different electrolyte modifications,[9] surface engineering approaches[15] as well as electrode support structures [16](current collector) have also been suggested to improve the electrochemical performance of alkali metal electrodes. However, to improve the performance of alkali metal anodes, it is important to also understand the mechanisms for performance enhancements with these different strategies. To enable this, the electrochemical responses during cell testing need to be accurately interpreted. The final part of the thesis is dedicated to investigating the voltage profile arising from different steps in the stripping and plating process of alkali metals.

1.1. Aim

The aim of this thesis is to aid the development of batteries with high energy densities by building a better understanding of the fundamental processes occurring at alkali metal electrodes during cycling. Particularly, the effect of altering the salt concentration on the cycling performance and the electrode interface is investigated. Further, the thesis aims to help improve the interpretation of the electrochemical signatures arising during the plating and stripping process.

Figure 1.1 schematically illustrates the different aspects of the alkali metal stripping and plating which are discussed in this work. (A) Electrolyte composition. (B) Interphase formation. (C) Electrochemical response of different parts of the stripping/plating process (illustration shows the example of nucleation).

Chapter 2 - Batteries

This chapter describes what a battery is and how it stores energy. Further, a brief review of the working principle for the Li-ion battery, the dominating (rechargeable) battery technology today, is given. The working principle of the Li-ion battery is put in relation to how batteries with alkali metal electrodes operate. Finally, the issues which need to be overcome to allow realization of rechargeable batteries with alkali metal electrodes in practice are discussed.

2.1. What is a battery?

A battery stores energy in chemical form, which can be converted to electricity through a spontaneous reaction. By definition, a spontaneous reaction is associated with a net reduction in Gibbs free energy of the involved chemical species. Neglecting any losses inside the battery, this energy can be transformed into electrical work.[17] When the battery is recharged, an external input of energy is instead needed to drive the reaction in the reverse direction.

In its most simple form, three essential components will be present in a battery (see figure 2.1), but often additional ones will also be needed. The battery has two electrodes, denoted as a negative and positive electrode, respectively, which are separated by an ionically conductive but electronically insulating electrolyte. This is often referred to as a cell. When the battery is discharged, an oxidation reaction takes place at one of the electrodes: [18]

$$R \rightarrow O^{n+} + ne^{-}, \qquad \text{Equation 2.1}$$

where, R is a species donating n electrons, e^{-}, to form an oxidized species O^{n+}. Because the electrolyte separating the two electrodes is electronically insulating, the electrons generated at the electrode are forced to pass through an external circuit before they can reach the other electrode. Here, electrons are instead consumed through a reduction reaction[18]

$$O'^{n+} + ne^{-} \rightarrow R'. \qquad \text{Equation 2.2}$$

For clarity, the prime denotes that the species in the reaction at the two electrodes (equations 2.1 and 2.2) need not be the same. To distinguish the two different electrodes, the naming convention in the battery field is to denote the electrode which is oxidized during discharge as the anode and the electrode which is reduced during discharge as the cathode.[19] When the battery is recharged, the reverse processes occur at each electrode.

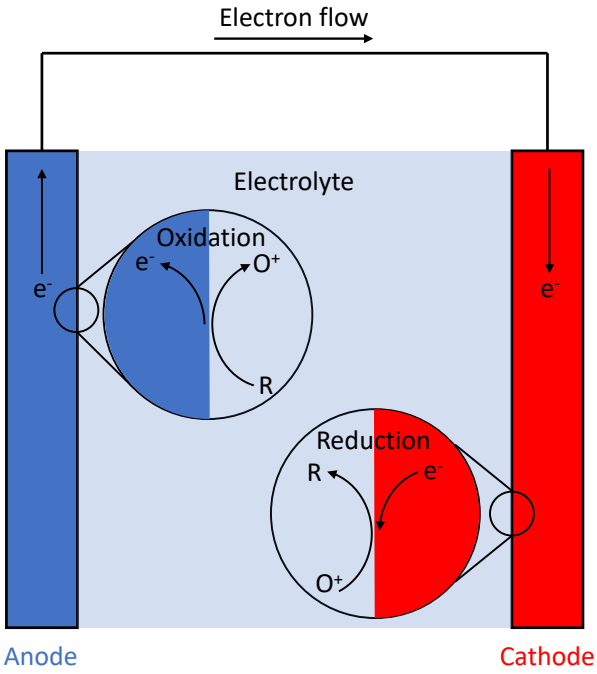

Figure 2.1. Schematic of the 3 fundamental components of a battery: The two electrodes, anode and cathode, and the electrolyte. During discharge an oxidation reaction occurs at the anode and a reduction at the cathode, producing a current in the external circuit.

2.1.2. Electrode potentials

During cell discharge, the electrons flow through the external circuit because the potential energy of an electron in the anode is higher than the potential energy of an electron in the cathode. To be able to predict in which direction a current will flow and how strong the driving force will be, electrochemists assign redox potentials to electrodes. The redox potential is set by the reaction taking place at the electrode surface and an electrode with a lower redox potential will spontaneously donate electrons to an electrode with a higher potential.

In practice, potentials always need to be measured as a difference with respect to another electrode. The potential difference between the two electrodes in a cell is often termed the cell voltage, E_{cell}, and can be determined as the difference between the redox potentials of each electrode:

$$E_{cell} = E_{cathode} - E_{anode} \qquad \text{Equation 2.3}$$

The potential across the electrodes of the battery, E_{cell}, can be linked to the difference in Gibbs free energy, ΔG, of the net chemical reaction produced in the cell:[17]

$$E_{cell} = -\frac{\Delta G}{nF}, \qquad \text{Equation 2.4}$$

where, n, is the stochiometric number of electrons exchanged during the reaction and F is Faraday's constant.

2.1.3. Energy stored

The power, P, delivered by a battery during discharge (or consumed when the battery is charged) can be described by:

$$P = V \cdot I, \qquad \text{Equation 2.5}$$

where V is the cell voltage, that is the difference in electric potential between the two electrodes, and I is the current passed through the cell. The total energy delivered during discharge (or that is needed to charge) can then be found by integrating this expression over the time, t, needed for (dis)charge.

$$\text{Energy} = \int_0^t V(t) \cdot I(t)\, dt \qquad \text{Equation 2.6}$$

Equivalently, this expression can be written in terms of the amount of charge a battery (or material) is able to store, i.e. the capacity, Q:

$$\text{Energy} = \bar{V} \cdot Q \qquad \text{Equation 2.7}$$

Where $\bar{V}$ denotes the average voltage. This expression highlights that high energy density can be attained both by using materials with high specific capacities (amount of charge stored per weight) or by using electrode materials that maximize the cell voltage.

2.2. Li-ion batteries

The rechargeable battery with the highest energy density on the commercial market today is the Li-ion battery. It is common to compare the working principle of a Li-ion battery with a rocking chair.[20] This alludes to the charge and discharge mechanism of the Li-ion host materials used as anode and cathode materials in Li-ion batteries. When the battery is charged and discharged, the Li-ions are shuttled between the anode and cathode, back and forth, like the rocking chair. This is visualized in figure 2.2 for a typical combination of electrode materials: graphite and $LiCO_2$. When the battery is charged, Li-ions are extracted from $LiCO_2$ at the cathode and inserted (intercalated) between the graphite layers at the anode. During discharge, the Li-ions move in the opposite direction, getting extracted from the graphite anode and inserted back into the lithium cobalt oxide cathode. The electrode reactions are summarized in equation 2.8 below[21]:

Cathode:	$\mathrm{Li}_{1-x}\mathrm{CO}_2 + x\mathrm{Li}^+ \leftrightarrow \mathrm{LiCO}_2$	Equation 2.8
Anode:	$\mathrm{Li}_x\mathrm{C}_6 \leftrightarrow x\mathrm{Li}^+ + x\mathrm{e}^- + \mathrm{C}_6$	

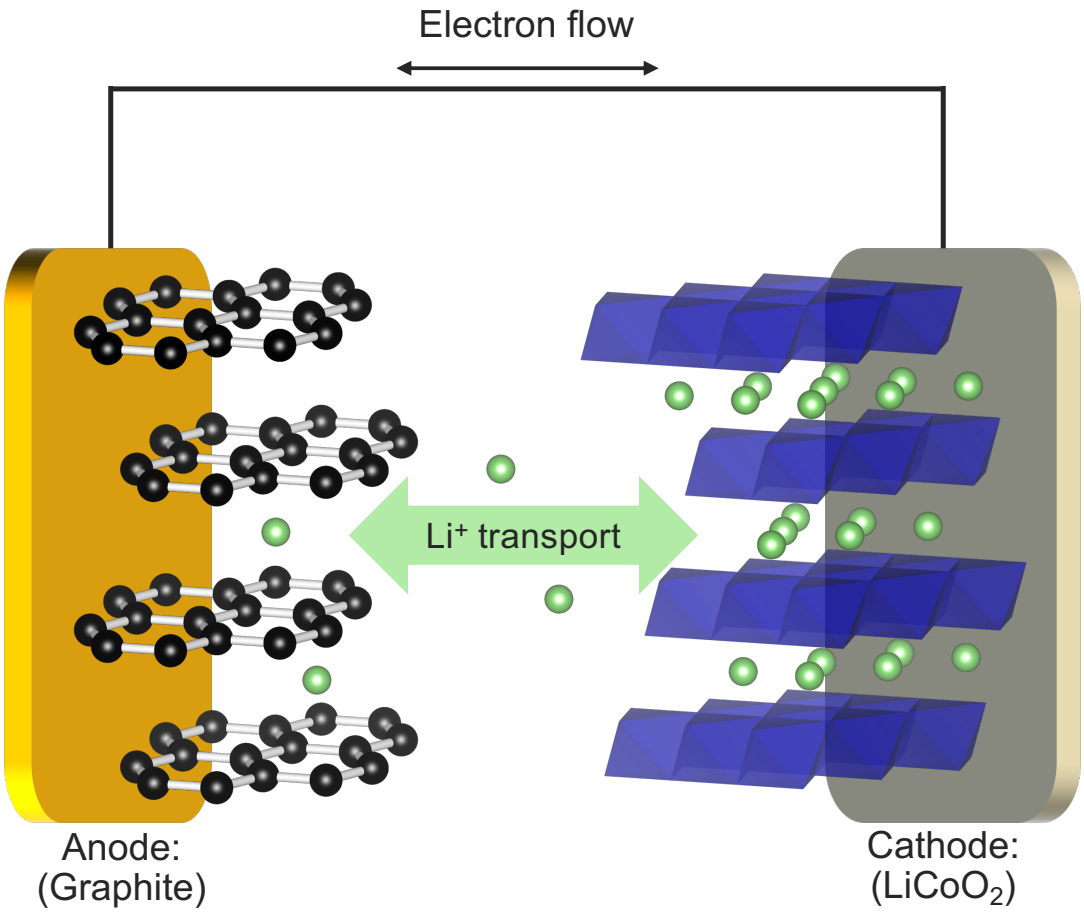

Figure 2.2. Rocking-chair mechanism of Li^+ in a Graphite-$LiCO_2$ lithium-ion battery. During charge, Li^+-ions (green) are extracted from $LiCO_2$ and intercalated into graphite. During discharge, the Li-ions deintercalated from the graphite and are inserted back between the CO_2-layers (blue) in $LiCO_2$.

Since Li-extraction and insertion do not cause any major changes to the structure of the host materials, excellent reversibility can be attained in Li-ion batteries [21]. For instance, the intercalation of Li into graphite only causes a 10% increase in the interlayer distance.[22] Further, electrolyte combinations that form stable passivation films (SEI-layers, detailed in section 2.3.2) on the anode surface during the first cycle help limit the side reactions which would consume active material and/or electrolyte.[23]

2.3. Alkali metal anodes

Stanley Whittingham pioneered the use of alkali metal anodes in batteries by designing a cell with a lithium metal anode and a Ti_2S cathode already in the 1970s.[24,25] Both Exxon Mobile and Moli Energy had commercial prototypes of lithium metal batteries in the late 1970s, however, the interest in lithium metal anodes quickly dropped after severe safety issues (described in section 2.4) were identified in these cells. [19] As Li-ion technology has matured, battery scientists have once again directed attention to lithium metal anodes to enable even higher energy densities. Especially after 2010, there has been a surge in the number of publications on the topic of lithium metal anodes.[3]

Instead of ion-intercalation into a host material, the lithium metal anode stores energy by plating lithium ions to form lithium metal and extracts energy by stripping metal from the anode (this process will be discussed in more detail in chapter 3). Since the cell can operate without a host material to hold the ions at the anode, lithium metal anodes store significantly more lithium compared to a graphite anode of the same weight. Another way to phrase this is that the theoretical specific capacity of lithium metal (3861 mAh/g) is much higher than that of graphite (372 mAh/g).[26] Lithium intercalation (into graphite) also happens at higher potentials than lithium plating,[2] which means that plating one lithium ion on the anode stores more energy than intercalating it into graphite. The combination of the lower reduction potential and the larger specific capacity give the cell a higher (theoretical) energy density compared to intercalation anodes. The problems with practically attaining this high energy density will be discussed in section 2.4.

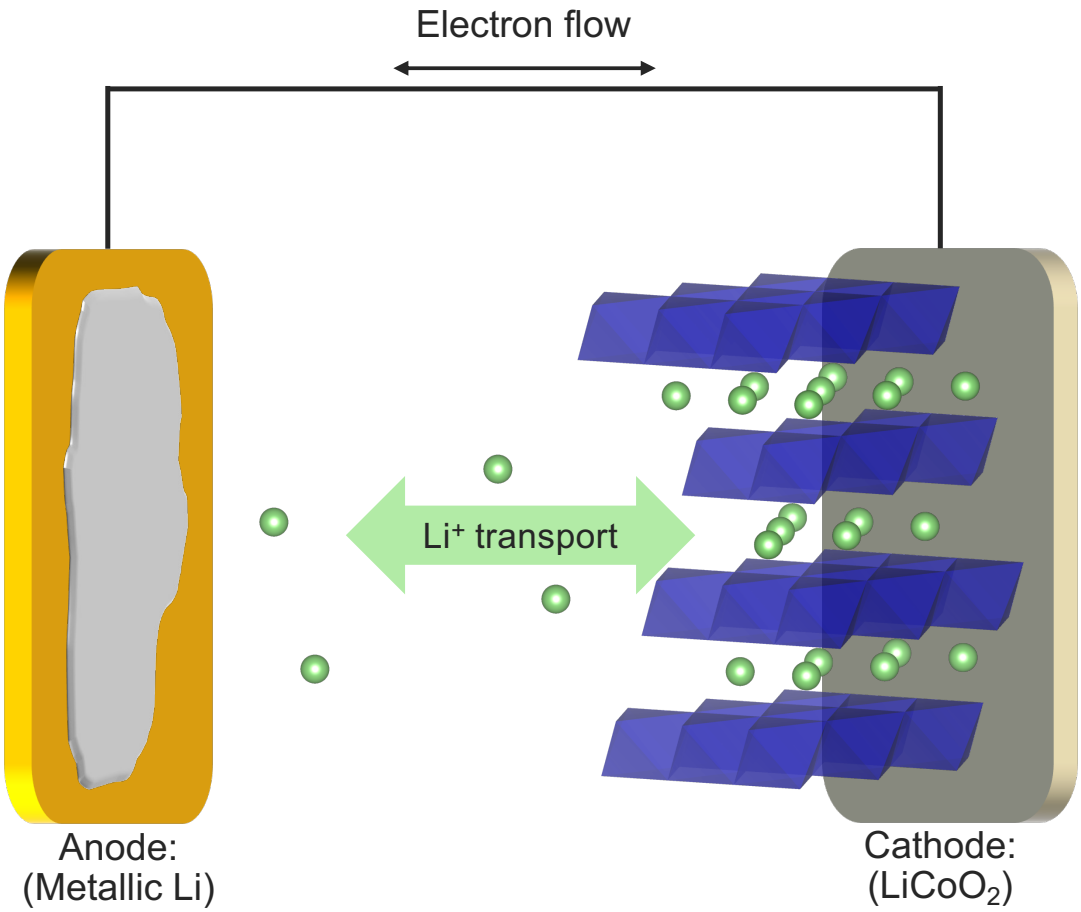

Figure 2.3. Working principle of a lithium metal battery with an insertion cathode (here illustrated with $LiCO_2$). During charge, Li^+-ions (green) are extracted from the cathode and plated on the anode, forming metallic Li. During discharge, the Li-ions are stripped from the anode and inserted back into the cathode.

2.3.1. Sodium and potassium metal anodes

The scarcity of Li has compelled battery researchers to look also for other high-energy electrode materials. The US geological survey estimated that global Li reserves total 89 million tons.[27] To put this number in context, the International Energy Agency suggests that carbon dioxide neutrality 2050 would require a fleet of 2 billion electric cars[28] and estimate that a car battery today contains 8.9 kg of lithium[29]. Based on these numbers, the global lithium reserves could be large enough to build roughly 10 billion cars. This suggests that global lithium resources might not be a threat to battery-powered vehicle production in the short term. Still, a heavy reliance of the transport sector on a scarce material with resources concentrated in a few places,[6] can be both politically and economically problematic. More than 50% of the Li produced globally today comes from Australia and more than 50% of the global Li reserves are concentrated in Bolivia, Chile and Argentina.[27]

The alkali metals Na and K have been explored as battery materials due to their high abundance, 2.3%[4] and 1.5%[5] in the earth's crust, several orders of magnitude more than Li (0.0017%[4]). Na-ion and K-ion batteries can be built with the same working principle as

the Li-ion battery.[30] Ions are transported back and forth between two different host materials with different intercalation/insertion potentials. However, since Na (23 u) and K (39 u) are much heavier elements than Li (6.9 u), Na-ion and K-ion batteries cannot match the energy densities of Li-ion batteries. However, the same case made for lithium metal anodes previously can be made more generally also for the other alkali metals. If the anode in an alkali-ion battery is exchanged for a metal anode, without changing the cathode, the theoretical energy density is always increased. This is because both the operational voltage of the cell and the capacity will be increased.[6,7] Theoretically, this type of change can result in an energy density increase of around 50%.[31] In practice, the numbers might be lower as excess anode material might be needed to prevent excessive capacity fading of the cell.

The energy density of alkali metal batteries is of course also heavily dependent on the cathode material used. If conversion cathodes are used instead of the insertion materials, the energy density of alkali metal batteries can be improved even further. For instance, sulfur cathodes have been extensively studied due to their very high theoretical capacities.[32–34] However, cathode materials fall outside the scope of this work.

2.3.2. The Solid Electrolyte Interphase

The high reactivity of alkali metal as well as the very reductive potentials that need to be applied to deposit alkali metal will cause electrolyte to break down at the surface of the electrode.[35] These decomposition products form of a thin, passivating surface layer on the electrode which is known as the solid electrolyte interphase (SEI)-layer.[12] The formation of a stable SEI-layer is essential to avoid continuous electrolyte consumption during cycling, which would inevitably lead to cell failure. Ideally, to enable stable and efficient cycling of metal anodes, the SEI-layer should be:[36]

- Electronically insulating, to passivate the electrode and prevent further electrolyte breakdown.
- Highly ionically conductive, to allow transport of the electrochemically active ions to the electrode, preferably without too much resistance (energy loss).
- Chemically stable, to maintain its structure over the cycle life of the cell.
- Mechanically strong and flexible, to avoid fractures and exposing fresh metal, aggravating side reactions and potentially creating hotspots for deposition.
- Spatially uniform, to avoid preferential deposition, resulting in dendritic deposition morphologies.[37]

To this date, several different structural models have been proposed to describe the SEI. However, the difficulty of investigating this very thin and sensitive film has not enabled conclusive evidence to determine which one most accurately represents the structure of the SEI. A mosaic model, describing the SEI layer as a mosaic of different electrolyte

decomposition products, has been proposed recognizing the importance of accounting for grain boundaries in the description of the impedance spectra of SEI-layers.[38] Several papers also suggest that the SEI has a bi- or multilayer structure, commonly described as an inner inorganic and an outer (porous) organic layer.[39–41] Other models of the SEI represent it as a double layer capacitor, wherein the charged components are held together via electrostatic forces.[42] Lately, cryo-transmission electron microscopy has also made direct imaging of the SEI-layer possible. Based on this type of experiments, the SEI-layer has been suggested to constitute mostly of amorphous components.[43] Further, it has also been suggested that SEI-layers are not compact films but swell in the presence of electrolyte.[44]

2.4. Problems in Metal anodes

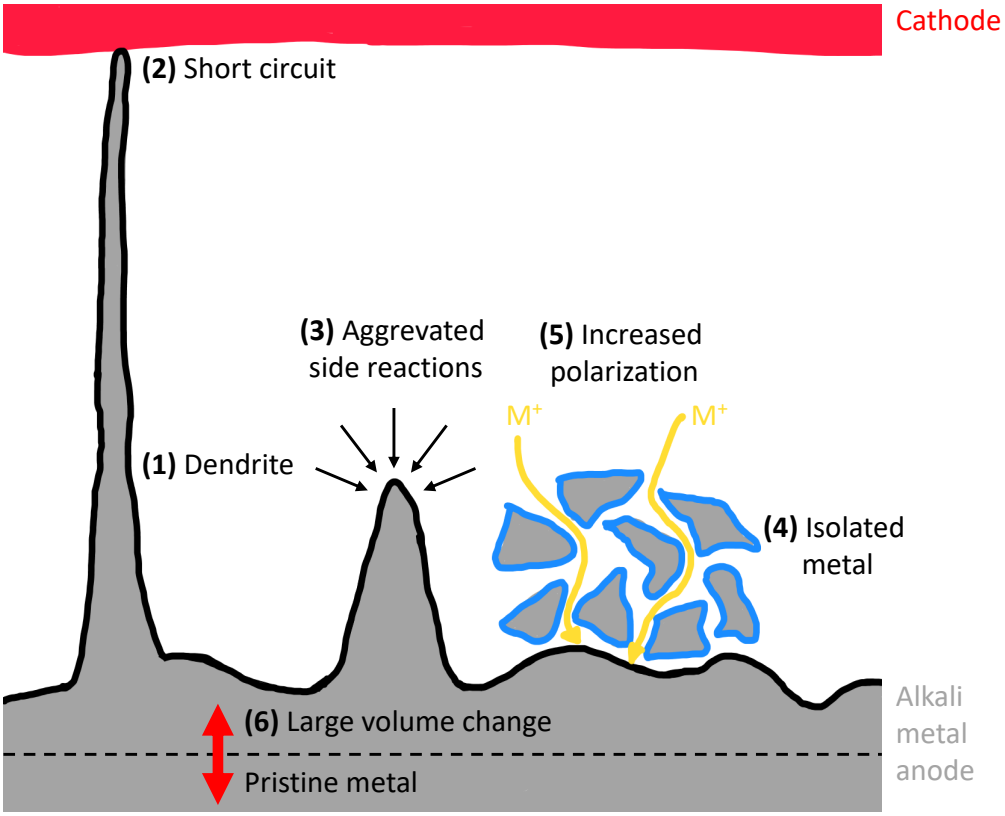

Figure 2.4. Schematic of problems in alkali metal anodes. Each type of problem is explained in the text. Inspired by [26]

Figure 2.4 schematically illustrates the most important issues currently hindering the application of alkali metal anodes. The electrochemical deposition of alkali metal tends to be inhomogeneous.[45] Although different types of growth modes can be identified, it is common to refer to all types of inhomogeneous deposits as dendrites (number 1 in figure 2.4).[14] The inhomogeneous deposition of alkali metals will be reviewed more thoroughly in section 3.4. Dendritic structures can cause problems in several ways. If dendritic structures are allowed to grow tall enough, they can penetrate through the separator to reach

the cathode, short-circuiting the cell (number 2 in figure 2.4).[46] This will inevitably lead to cell failure but can also create serious safety problems.[47]

The inhomogeneous deposition will also expose larger surface areas of metal to the electrolyte. Larger surface areas will lead to aggravated side reactions and invariably both more electrolyte consumption and loss of active material (number 3 in figure 2.4).[26] The active material can also be lost through the formation of electronically isolated, or 'dead' metal, during the plating/stripping process (number 5 in figure 2.4).[48] For instance, this can occur if the base of a dendritic structure is stripped before the top, leaving the top part electronically disconnected from the bulk electrode. A layer of 'dead' metal and/or electrolyte decomposition products can also build up at the anode surface, giving lithium ions a more tortuous pathway to the anode. This will increase the electrode polarization during plating/stripping (number 5 in figure 2.4).[48] Finally, the large volume change that the anode goes through during plating and stripping will strain and possibly crack the surface film on the alkali metal surface, exposing unreacted metal to the electrolyte.[49] This behavior can both increase electrolyte consumption through side reactions and drive uneven metal deposition.[49]

2.4.1. Reversibility

Several of the problems discussed in the previous section limit the reversibility of the alkali metal stripping/plating reaction. One way to quantify the reversibility of a cell is to determine the Coulombic efficiency (CE). This is a measure of what fraction of the electrons spent charging the cell can be recovered at discharge:

$$\mathrm{CE} = \frac{\text{Discharge capacity}}{\text{Charge capacity}} \qquad \text{Equation 2.9}$$

This parameter is crucial for determining how much excess electrode material needs to be used to give the cell the desired cycle life. It is common to define the end of life for a battery when it retains only 80% of its initial capacity.[3] Figure 2.5a shows the capacity retention for cells with different CEs and no excess electrode material. Without excess electrode material, cells with a CE of 99.9% would only have a cycle life of around 200 cycles. To improve the cycle life, excess electrode material can be used, see figure 2.5b. With 100% excess electrode material, a cell 99.9% CE would instead survive for more than 1200 cycles. The excess material will, however, diminish the energy density of the cell. This highlights the importance of attaining high reversibility for the metal stripping/plating process to allow cells with metal anodes to have both high energy densities and acceptable cycle lives.

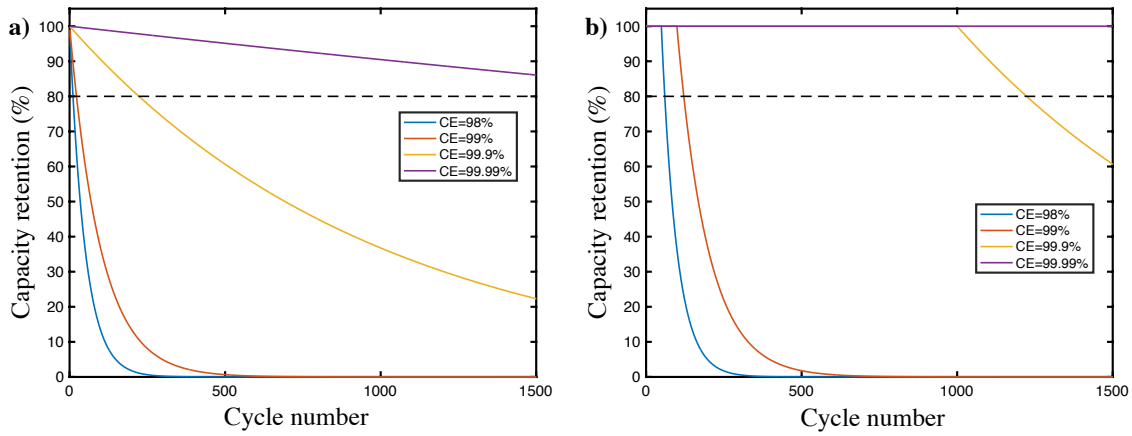

Figure 2.5. Capacity retention for different Coulombic efficiencies in a cell with a) no excess of active material. b) 100% excess material. Dashed black lines mark the 'end-of-life' at 80% capacity retention.

Through extensive efforts to develop the electrolytes used for lithium metal batteries, the reversibility of lithium metal anodes has improved from around CE=80% in 1974 to well above 99% in several electrolytes today, with the highest reported CE around 99.9%.[50] Also for Na-anodes, CEs of 99.9% have been reported,[51] while the CEs of potassium metal stripping/plating are generally lower, to my knowledge, the highest reported CE value is 99.6%[52]

Chapter 3 - Metal stripping and deposition

This chapter is dedicated to the fundamental physics and electrochemistry governing the stripping and plating process of alkali metals from liquid electrolytes.

3.1. Overpotential

The potential, E, which is required for some electrochemical reaction to occur will always deviate from the equilibrium potential, E_{Eq}, predicted from the change in Gibb's free energy (equation 2.4).[53] This difference is known as the overpotential, η:

$$\eta = E - E_{Eq} \qquad \text{Equation 3.1}$$

and can be associated with energy barriers and processes involved in the electrochemical reaction.[18] By changing the applied (over)potential, the reaction rate can be altered. [54] Equivalently, if the reaction rate (current) is instead fixed, changes in the overpotential can help us learn about the energy barriers associated with different steps of the reaction(s).

3.2. Deposition

For metal deposition, several key steps need to occur, all associated with an overpotential. These steps are schematically illustrated in figure 3.1. (1) *Mass transport*. The reactants need to diffuse through the electrolyte and the SEI-layer to reach the electrode. [55,56] (2) *Charge transfer*. The reduction of metal ions on the surface of the electrode is associated with an energy barrier that needs to be overcome for the reaction to take place.[57] (3) *Nucleation*. Metal atoms adsorbed on the electrode surface need to nucleate to form a new phase.[57] In the following subsections, these different processes occurring during the metal electrodeposition will be described in more detail.

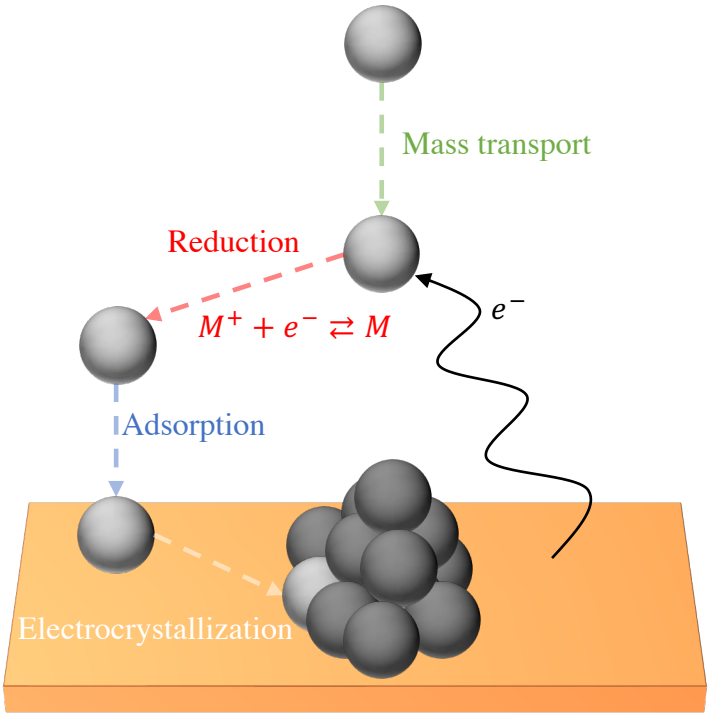

Figure 3.1. Key steps for metal deposition from a liquid electrolyte.

3.2.1. Mass transport

Mass transport can occur through 3 different mechanisms, convection/stirring, electrical migration or diffusion.[18] This can be summarized using the Nernst-Planck equation, describing the flux, J, of an arbitrary species j in solution:[54]

$$\boldsymbol{J}_j = -D_j \boldsymbol{\nabla} C_j - \frac{z_j F}{RT} D_j C_j \boldsymbol{\nabla} \phi + C_j \boldsymbol{v}, \qquad \text{Equation 3.2}$$

where, D, C and z, are the diffusion coefficient, concentration, and dimensionless charge of an ionic species. ϕ and $\boldsymbol{v}$ are the potential and the convection velocity. The first term in equation 3.2 represents the diffusion due to a concentration gradient, the second one the migration current and the last term the mass transport due to convection. In battery science, the contribution of convection is frequently neglected.[57,58] However, for large currents, it may play an important role.[59]

In equilibrium, the net current through an electrochemical cell will be 0. According to the Nernst Einstein equation (having neglected convection), this means that the concentration of ions has been distributed in the cell to compensate for any gradient in the electric potential. Now, when a current is applied, ions will be consumed at one electrode and produced at the other, creating a concentration imbalance, which will drive mass transport through diffusion. In most batteries, this diffusion process is the main mode of mass transport although migration also plays a part.[18] The use of a supporting electrolyte, with a large

concentration of a salt that does not participate in the electrode reactions, can eliminate the contribution of migration to the mass transport.[60]

3.2.2. Charge transfer

The redox reaction occurring at the electrode in this work is a one electron transfer process described by the general reaction

$$M^+ + e^- \rightleftarrows M, \qquad \text{Equation 3.3}$$

where some ion, M^+, in solution, is oxidized to form a metal, *M*, atom on the electrode. This metal atom can of course also be oxidized again and return a metal ion to the electrolyte solution. In equilibrium, when no net current is produced, the forward and backward reactions are happening at the same rate. However, by applying a potential, the direction and rate of this reaction can be controlled. This is described by the Butler-Volmer equation, which links the overpotential to the net current. Here, the equation is adapted to describe the reduction of alkali metal-ions (M^+) at the electrode-electrolyte interface to form alkali atoms (adsorbed on the electrode):[57]

$$j = j^0 \left[\frac{C_{M^+}^S}{C_{M^+}^b} \exp\left(\frac{\alpha F}{RT}\eta\right) - \frac{C_M^S}{C_M^b} \exp\left(-\frac{\beta F}{RT}\eta\right) \right] \qquad \text{Equation 3.4}$$

where j^0 is the exchange current density, $C_{M^+}^S$ and $C_{M^+}^b$ are the concentrations of metal ions at the surface and in the bulk electrolyte, respectively. Similarly, C_M^S and C_M^b are the surface and bulk concentrations of metal atoms. α and β are the anodic and cathodic transfer coefficients. The first term in equation 3.4 describes the reaction progressing in one direction (reduction of metal ions), and the second term describe the reaction progressing in the other direction.[54] Neglecting the concentration effects, this equation is plotted in figure 3.2.

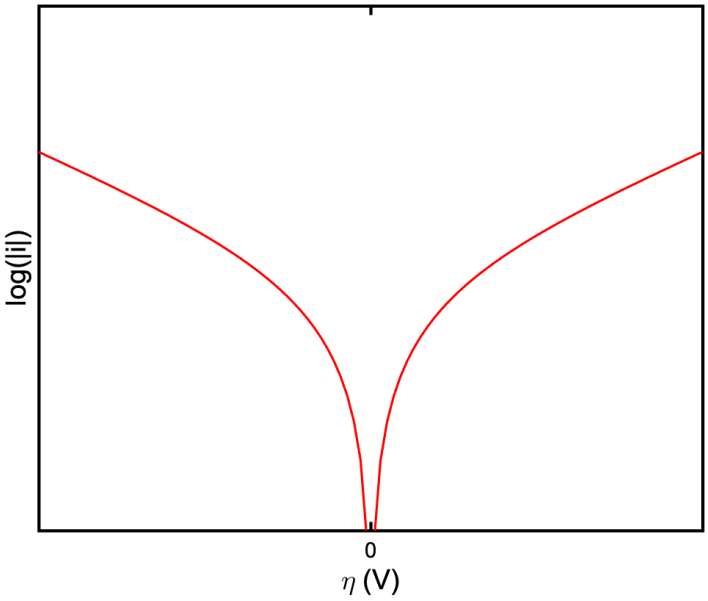

Figure 3.2. Charge transfer overpotential for different currents, illustrated by the Butler-Volmer equation (equation 3.4), neglecting any concentration effects, with transfer coefficients $\alpha = \beta = 0.5$.

3.2.2. Nucleation

Finally, the adsorbed atoms on the surface of the electrode will need to nucleate to form a new phase. The Gibbs free energy change during nucleation on a substrate, ΔG_{Nuc}, (heterogeneous nucleation) has three different contributions:

$$\Delta G_{Nuc} = \Delta G_{Bulk} + \Delta G_{S,Base} + \Delta G_{S,\mathrm{El}}, \qquad \text{Equation 3.5}$$

the energy reduction for atoms in the bulk crystal, ΔG_{Bulk}, and the surface energies of the base of the nuclei, $\Delta G_{S,Base}$, (interface between nuclei and substrate) and the part of the nuclei in contact with the electrolyte $\Delta G_{S,El}$. More explicitly, these terms can be expressed as:[61]

$$\Delta G_{Nuc} = \mathrm{V}\Delta G_V + \mathrm{A}_1\gamma_1 + \mathrm{A}_2(\gamma_2 - \gamma_0) \qquad \text{Equation 3.6}$$

where ΔG_V is the Gibbs free energy of supersaturation, A_1 and A_2 are the areas of the nuclei in contact with the electrolyte and substrate, respectively. γ_1 and γ_2 are the corresponding surface energies, and γ_0 the surface energy between electrolyte and substrate. It is possible to show that for a spherical cap shaped nuclei (see inset of figure 3.3a) with some contact angle, θ, with the substrate, the Gibbs free energy change during nucleation can be written as:[62]

$$\Delta G_{Nuc} = \left(-\frac{4}{3}\pi r^3 \Delta G_V + 4\pi r^2 \gamma_1\right)\left(\frac{2 - 3\cos\theta + \cos^3\theta}{4}\right) \qquad \text{Equation 3.7}$$

This expression is plotted for an arbitrary contact angle in figure 3.3a. The graph illustrates that for small nuclei, there is an energy cost associated with the growth of the nuclei, until it

reaches a certain, critical radius (r^*) after which further growth is energetically favorable. The energy needed to form a nucleus of the critical radius will constitute an energy barrier for nucleation. This energy barrier arises due to the competition between the cost of the surface energy of the nucleus, and the lower energy of atoms in the bulk crystal lattice. Since the bulk energy term has an r^3-dependence, while the surface energy term grows with the square of the crystal radius, the bulk energy gain eventually dominates for large enough radii. To overcome the energy barrier associated with the nucleation and form a new phase, it is necessary to apply an overvoltage, [63,64] illustrated in figure 3.3b.

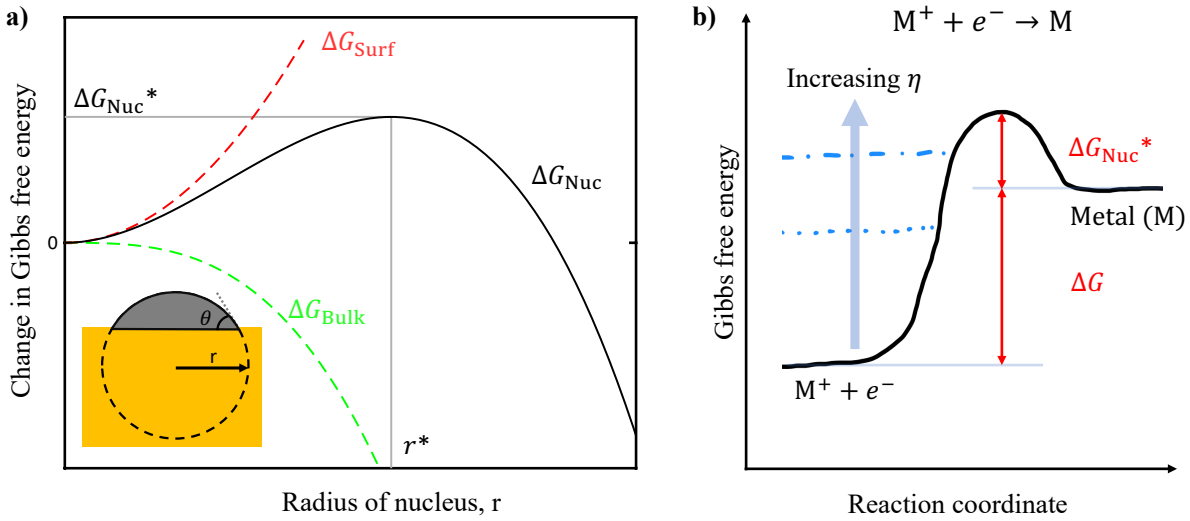

Figure 3.3. Energy barriers in electrodeposition. a) Gibbs free energy change during nucleation of a spherical cap nucleus (with a fixed contact angle) on a substrate. b) Energy barrier associated with nucleation and the influence of overpotential. Redrawn from.[65]

3.3. Stripping

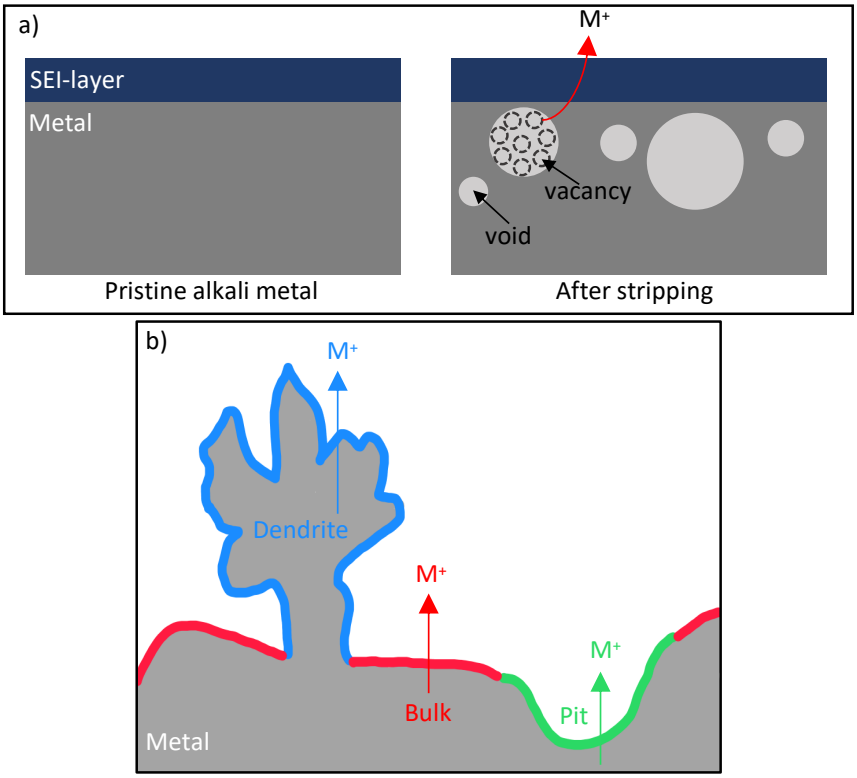

Figure 3.4. Stripping from an alkali metal electrode. a) Void formation during stripping. Inspired by [66]. b) Different parts of the metal anode, typically associated with different stripping resistances, illustrated with different colors. Redrawn from [67]

In principle, during the stripping process, the same steps which were described for plating/deposition in section 3.2 need to occur, but in the reverse order. However, during stripping no nucleation takes place. First, charge transfer needs to occur, metal ions in the bulk electrode need to be oxidized to produce metal ions. Then, the metal atoms need to diffuse through the electrode and the SEI to reach the electrolyte (mass transport).

The electrode morphology is of course dictated not only by the plating process, but also by the stripping process. For instance, when metal atoms are stripped from the electrode, vacancies in the bulk metal will be created (figure 3.4a). If enough vacancies are formed, voids will be created inside the electrode.[66] For high enough stripping-rates, this void formation process can trigger a local breakdown of the SEI-layer, resulting in the formation of a pit in the electrode. [66] Further, the resistances associated with different diffusion pathways for the stripped ions will influence where on the electrode metal is stripped from. For instance, lithium diffusion in bulk metal is usually much lower than the diffusion through the SEI layer, which leads to pits being more likely to form close to grain boundaries where the ions can diffuse faster.[66] The different types of metal morphologies are prone to exhibit different resistances during the stripping process, as illustrated in figure 3.4b. Since the alkali metal is very reactive, there will already be a native oxide layer on its surface before the cell cycling starts,[12] and mass transport through this layer will be

associated with some resistance. Electrochemically deposited structures on the other hand will form a surface layer only from the decomposition of electrolyte, typically giving another resistance for stripping from the deposit compared to the bulk metal. Finally, the pitted electrode surfaces can have yet another type of interfacial layer/SEI.

3.4. Explanations for dendrite growth

The electrochemical formation of a metal from ions in a solution is not unique to the battery field. Different types of electroplating have been studied for more than 200 years.[68] Several different metals like copper, tin, lead and various different alloys, have been plated this way, often from aqueous electrolytes.[69] This process carries many similarities with the plating of alkali metal in a battery. For instance, also in conventional electroplating, dendrite growth is a known problem. Therefore, models for understanding dendrite growth in conventional electroplating have often been applied to understand the uneven deposition morphology of alkali metals. It is important to stress, however, that there are several key differences between alkali metal stripping and plating in batteries and the electrodeposition of for instance Cu. Alkali metals require nonaqueous electrolytes to be used and spontaneously form SEI-layers on their surfaces.[68] This needs to be considered to understand the alkali metal plating process. Further, for metal batteries, the deposition and stripping of metal are repeated over several cycles.

3.4.1. Diffusion limited current and Sand's time

Metal electrodeposition can be seen as a mass transport problem. Metal ions will be generated at one electrode, and consumed at the other electrode by a reduction process depositing them as metal atoms.[3] To sustain a certain current over time, the ions need to be transported sufficiently fast from the electrode where they are generated to the electrode where they are consumed. Neglecting the effect of convection, the maximum current density which can be sustained based on the effect of ion diffusion can be estimated from [3,70]

$$J^* = \frac{2ec_0D}{t_aL}, \qquad \text{Equation 3.8}$$

where, e is the elementary charge, c_0 the bulk salt concentration, D the ambipolar diffusivity for the ions in solution[1], t_a the anionic transport number and L the inter-electrode separation. This current limit is usually denoted as the diffusion-limited current density, J^*, above which the surface concentration of metal ions at the anode will fall to 0.[71]

[1] $D = \frac{D_a\mu_c + D_c\mu_a}{\mu_c + \mu_a}$, where D_a and D_c are the anionic and cationic diffusion constants. μ_a and μ_c are the anionic and cationic mobilities.

Fractal growth can be induced when the surface concentration of metal ions reaches 0. Above the diffusion limiting current density, the ions at the surface of the anode are consumed faster than they can be transported there. The time it takes for the surface concentration of metal ions to reach 0 is referred to as the Sand's time.[72,73] For an electrolyte containing only one cationic and one anionic species, which will be the case throughout this thesis, the Sand's time can be calculated from:

$$t_{Sand} = \pi D \frac{(z_c c_0 F)^2}{4(J t_a)^2} \qquad \text{Equation 3.9}$$

where z_c is the dimensionless charge of the cation (1 for alkali ion deposition) and J is the applied current density. After the Sand's time, electroneutrality will be broken close to the surface of the electrode and locally charged regions created. This will preferentially drive deposition to protrusions in the surface or dendrites,[6] a mechanism commonly used to explain dendrite growth for copper deposition from an aqueous solution. [72,74] However, with the electrode separations and current densities reported for most experiments on alkali metal deposition in batteries, the diffusion limited current suggests that the surface concentration will never fall to 0.[75] This limits the utility of Sand's time as an explanation for dendrite growth in alkali metal anodes, which can be illustrated by plotting the limiting current density (equation 3.11) for different electrode separations for a common lithium electrolyte, see figure 3.5. It is possible, however, that the diffusion limited current above is a too idealized way to estimate the magnitude of the current density that can be sustained by diffusion. Mistry and coworkers argue that uneven lithium deposits will trap electrolyte at the electrode surface, which can lead to ion depletion even at currents below the estimated limiting current density for the cell.[75] Additionally, already ion concentration gradients at the electrode surface can still impact the deposition morphology.[58]

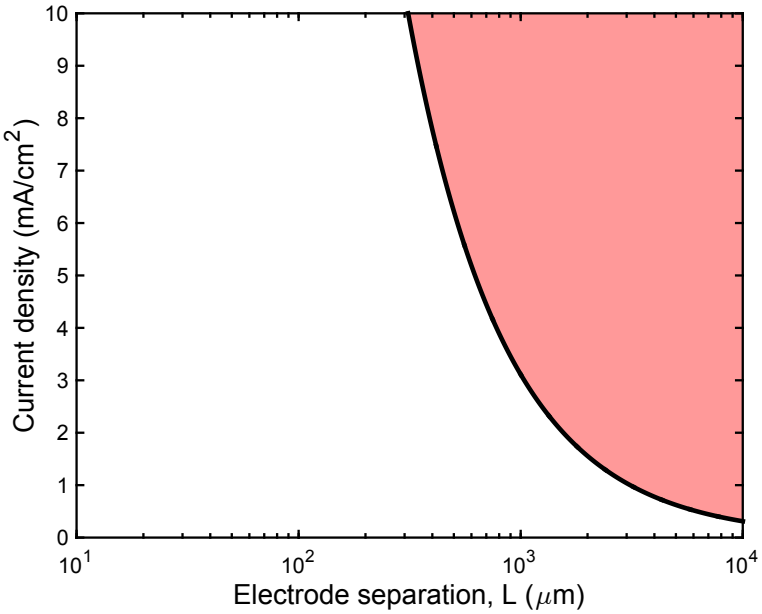

Figure 3.5. Conditions under which dendrite growth is predicted due to ion depletion at the surface of the electrode (red area). Plot based on equation 3.8 for a typical lithium electrolyte (1M $LiPF_6$ in EC:DMC). A diffusion coefficient, $D = 1 \cdot 10^{-6}$ cm^2/s and the anionic transference number $t_a = 0.62$ was used.[72]

3.4.2. Mechanically weak separators

It has been suggested by Monroe and Newman[76] that a mechanically strong separator can prevent uneven deposition. This idea has inspired the use of solid-state electrolyte or separators to stabilize alkali metal deposition.[8] For instance, the company QuantumScape, currently attempting to design lithium metal batteries for commercial use utilize this strategy by using a ceramic separator.[77] Further, with a similar argument, a mechanically strong interfacial layer at the electrode surface (artificial SEI) can reduce the dendritic growth.[78]

3.4.3. Nonuniform interphase

A non-uniform interphase at the electrode has also been suggested as the precursor for nonuniform deposition.[8] The SEI that forms on lithium metal has been confirmed to be chemically non-uniform, which will tend to induce a non-uniform current density.[49] The uneven deposition can also induce stress on the SEI-layer, possibly causing cracks to further aggravate the uneven deposition.[49]

Chapter 4 - Theory & Experimental

This chapter will explain the working principles of the experimental methods used within the thesis. These include different types of electrochemical cycling as well as Raman spectroscopy and neutron reflectometry.

4.1. Electrochemical methods

The electrochemical methods can be divided into two different categories. Either, the current passed through the cell is controlled and the voltage response of the cell is measured (see section 4.1.1) or the other way around (see section 4.1.2).

4.1.1. Galvanostatic cycling

In a constant current experiment, a potentiostat or galvanostat is used to maintain a fixed current flowing between the electrodes of the cell and the potential that needs to be applied to maintain the set current is measured.[54] This kind of experiment is frequently used for evaluating battery materials and full cells, to ascertain e.g. their cycle life or rate capability.

Two different categories of cell configurations are used to test the stability and reversibility of the metal anodes, see figure 4.1. The first type of cell, a *symmetric cell* where both electrodes are alkali metal foils, is often used to analyze the compatibility between an electrolyte and a metal anode (figure 4.1a). For instance, the tendency for a cell to short circuit or the evolution of the interfacial resistance of the electrodes during cycling can be studied. [13,14,48,67] In an *asymmetric cell*, an alkali metal foil acts as an ion reservoir and counter electrode (CE) while the working electrode (WE) is a non-reacting metal, typically copper (figure 4.1b). The efficiency of the metal stripping/plating in an electrolyte can be assessed by repeatedly plating alkali metal on the copper surface and stripping it again.[79,80]

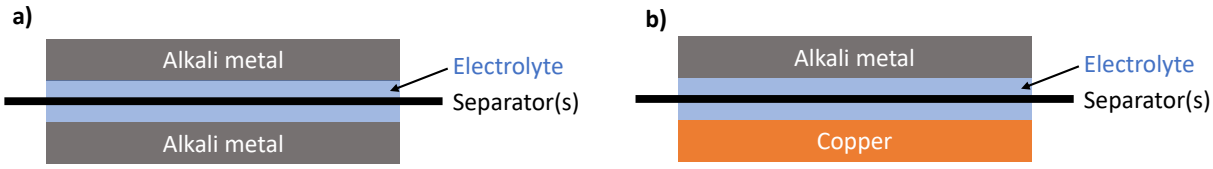

Figure 4.1. Cell configurations used for the analysis of metal anodes. a) Symmetric cell, using two alkali metal electrodes. b) Asymmetric cell with one copper electrode and one alkali metal electrode.

4.1.2. Cyclic Voltammetry

Cyclic voltammetry (CV) is used to investigate the reduction and oxidation potentials of different reactions.[81] The potential of the working electrode is increased/decreased at a constant rate, while the current flowing between the counter and the working electrodes in response to the applied potential is monitored. Usually, the potential is scanned in a cyclic

fashion between two values. An illustration of a CV-curve is given in figure 4.2, where a CV-experiment has been simulated for a reversible redox reaction. In this experiment, a negative scan from a starting potential to a lower cutoff potential is first performed and then a positive scan returns the potential back to the initial value. As the electrode potential approaches the equilibrium potential of the redox reaction, a current starts to flow. However, the reaction giving rise to the current eventually depletes the interface between electrode and electrolyte of reactants, leading to a decay of the current to some lower value set by the rate at which reactants can be transported to the electrode. This gives rise to a characteristic peak in the current vs potential plot, with some offset from the reduction potential.[54] In the positive scan, the reverse redox reaction takes place and gives rise to a peak, which is shifted to higher potentials. The standard reduction potential can be determined as the average between the peak values seen in the positive and negative scans, marked by a dashed line in figure 4.2.

A CV-scan can also shed light on the nature of the transitions. For instance, the reversibility of a reaction can be determined as a peak should be obtained in both the negative and positive potential scans. If a peak is found only in one scan direction the process is irreversible.

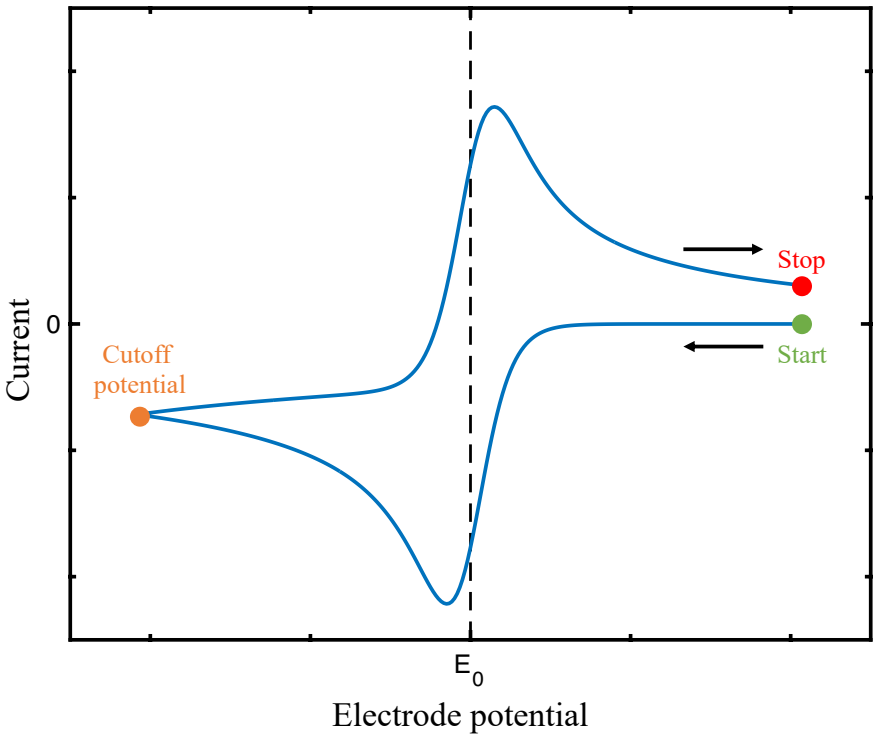

Figure 4.2. Schematic CV-curve for a reversible redox reaction with standard potential E_0. The potential of the working electrode is linearly decreased from a starting value (green point) to a cutoff potential (orange point) and then increased again to return to the initial potential.

4.1.3. Three-electrode and two-electrode configurations

For battery testing, it is common to use a two-electrode cell (figure 4.3a) and in this case, the current will flow between a counter electrode (CE) and a working electrode (WE). Since it is only possible to measure electrode potentials relative to another electrode,[82] this configuration only allows the potential difference between WE and CE to be determined. This can be problematic as currents will polarize both electrodes, and no independent measure of the potential of either WE or CE can be obtained. [83]

To separate voltage changes arising from processes occurring at the working and counter electrodes, a reference electrode (RE) can be introduced in the cell (figure 4.3b). This electrode will only carry a very small current necessary to measure the potential, minimizing its polarization. If the RE has a stable potential, the potentials of the WE and CE can be determined independently in this configuration, denoted as a three-electrode cell.

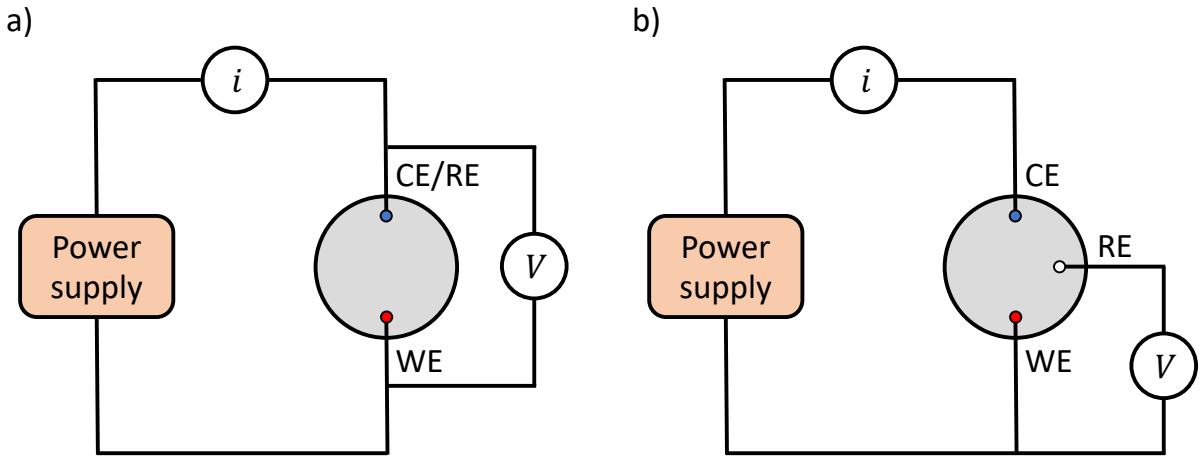

Figure 4.3. Measurement configurations. a) Two-electrode measurements. b) Three-electrode measurements. Redrawn from [82].

4.2. Raman Spectroscopy

When light impinges on a material, most photons that are scattered from an ion/molecule will have the same energy before and after the scattering event, which is called elastic scattering. However, roughly 1 in 100 000 photons will be scattered inelastically and instead exchange energy with the molecule/ion. This type of scattering is called Raman scattering and constitutes the basis for the technique Raman spectroscopy. In a Raman spectrometer, a sample is illuminated with monochromatic radiation and the energies of inelastically scatted photons are analyzed. Each photon energy shift, ΔE, corresponds to the energy difference between two quantized energy states in the molecule/ion.[84]

Typically, in Raman spectroscopy, the photon energy shifts are associated with the excitation or deexcitation of vibrational states of different ions or molecules. [84] As an example, consider the molecule CCl_4. The atoms in this molecule can vibrate in several different ways, one has been exemplified in figure 4.4a. In what is known as a symmetric

stretching vibration, the Cl atoms (green) alternate between moving away from and towards the C atom at the center of the molecule (black). The vibrational energy can be described by the formula

$$E = h\nu_m, \qquad \text{Equation 4.1}$$

where h is Planck's constant and ν_m, the characteristic vibrational frequency of the motion. The different scattering events that are possible when a photon hits a molecule/ion are shown in figure 4.4b. An incident photon hitting a molecule in its ground state, E_0, will be excited to a virtual state (dashed line), before the virtual state is de-excited, sending out a scattered photon. When incident and scattered photons have the same energy, the event is called elastic or Rayleigh scattering. The scattered photon can also have lower energy than the incident photon, leaving the molecule in an excited vibrational state, known as Stokes scattering. Finally, some molecules are already in an excited vibrational state before the scattering event. In this case, the vibration can be deexcited, giving rise to a scattered photon with higher energy than the incident photon, known as anti-stokes scattering. The energy shift involved in the stokes and anti-stokes scattering is characteristic of the vibration that has been (de)excited.

Different chemical bonds or functional groups vibrate with different frequencies, which can be explained by using a spring, with a spring constant K, to describe the bond between two atoms of mass m_1 and m_2. Solving the equations of motion for this system, the atoms can be seen to vibrate with a frequency

$$\nu_m = \frac{1}{2\pi}\sqrt{\frac{K}{\left(\frac{m_1 m_2}{m_1 + m_2}\right)}}. \qquad \text{Equation 4.2}$$

As different chemical bonds have different strengths and masses of the involved species, already this very simple model predicts that different functional groups will result in different Raman shifts. In this thesis, Raman spectroscopy is used to understand the solvation structures in different electrolytes. Solvation of an ion will delocalize electrons participating in the covalent bonds of solvent molecules.[85] This will modify the strength of the covalent bond, which based on the model above will change the vibrational frequency and thus also the position of the Raman band.

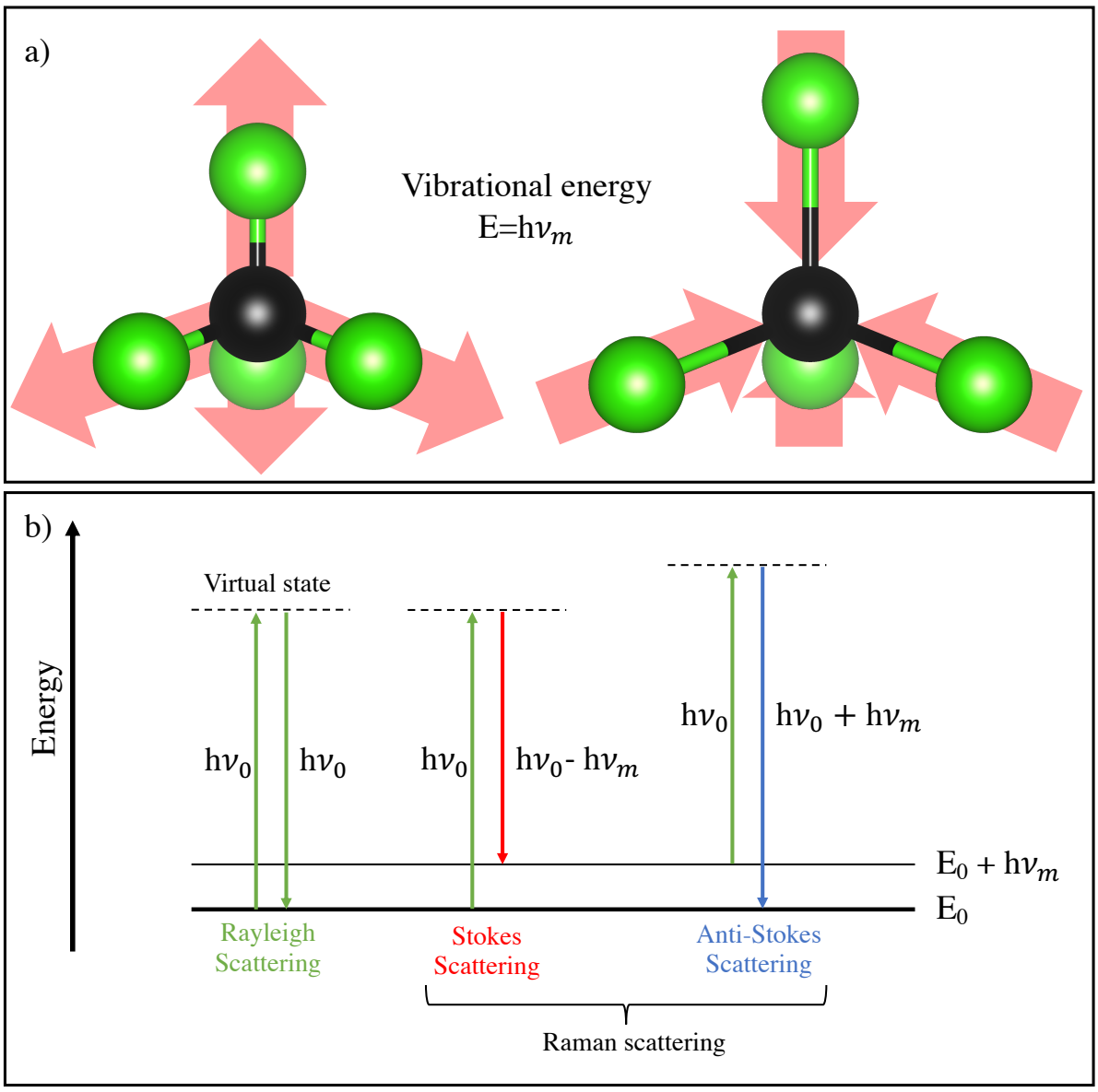

Figure 4.4. Principles of Raman spectroscopy. a) Example of a symmetric stretch vibrational mode in CCl_4. b) Schematic energy diagram describing the difference between elastic (Rayleigh) scattering and inelastic (Raman) scattering.

4.3. Neutron Reflectometry

Reflectometry is a common tool for the characterization of films with thicknesses varying from fractions of a nanometer to hundreds of nanometers.[86] The technique has frequently been used for depth profiling of samples ranging from biological membranes or surfactants to thin film depositions, but can also be used to characterize electrochemical interfaces like the SEI-layer.[87,88] During a measurement, the reflectivity is measured, that is the intensity ratio between the beam incident on a surface and the reflected beam. Specifically, *specular*, or mirror-like reflection is used in this thesis, where the incidence angle and reflection angle are the same (schematically illustrated in figure 4.5). In an experiment, the specular reflectivity is monitored as a function of the momentum transfer vector, Q:

$$Q = \frac{2\pi}{\lambda} \sin\theta, \qquad \text{Equation 4.3}$$

where λ is the wavelength and θ is the incidence angle. In practice, Q is varied either by rotating the sample to change the incidence angle or by letting the wavelength of the beam vary.

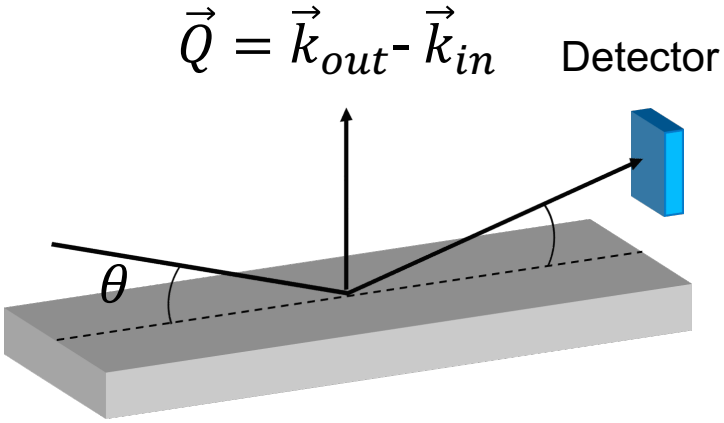

Figure 4.5. Schematic of a reflectometry measurement. An incident beam is specularly reflected from a surface and the intensity of the reflected beam is detected.

The material parameter that governs the reflection of x-rays or neutrons is the scattering length density (SLD), ρ. The SLD is determined by the composition and density of a material through the following equation: [89]

$$\rho = \sum_i b_{c,i} N_i \qquad \text{Equation 4.4}$$

where $b_{c,i}$ is the scattering length and N_i the number density of element i. At an interface where the SLD changes, part of the beam will be reflected, and part of the beam will be transmitted. How strong the reflection is will depend on incidence angle, SLD-contrast at the interface as well as the wavelength. [90]

Consider a layer in a sample (figure 4.6a) with a different SLD compared to its surroundings. Both at the interfaces above and below this layer, part of the beam will be reflected. The parts of the beam reflected at the top and bottom interfaces will have different path lengths to reach the detector, set by the layer thickness, d, and incidence angle, θ, of the beam. These reflections will interfere constructively or destructively with each other at the detector, depending on the resulting phase difference. This gives rise to an interference pattern when reflectivity is plotted against Q (figure 4.6b), which will encode information about the layer, such as layer thickness, SLD and interfacial roughnesses. At small Q, there is a plateau due to the total reflection of the incident beam when the incidence angle is below the critical angle, whereas a fringe pattern emerges for higher Q. The valleys of the fringe pattern arise due to destructive interference and the peaks due to

constructive interference between parts of the beam reflected at the different interfaces. The width of the fringe is proportional to the thickness of the layer and the height reflects the SLD contrast at the interfaces.[90] Similarly, the roughness of the interfaces will also impact the reflectivity curves. A rougher interface will lead to a steeper falloff of the reflectivity vs Q, and dampen the fringe amplitude at higher Q.[86]

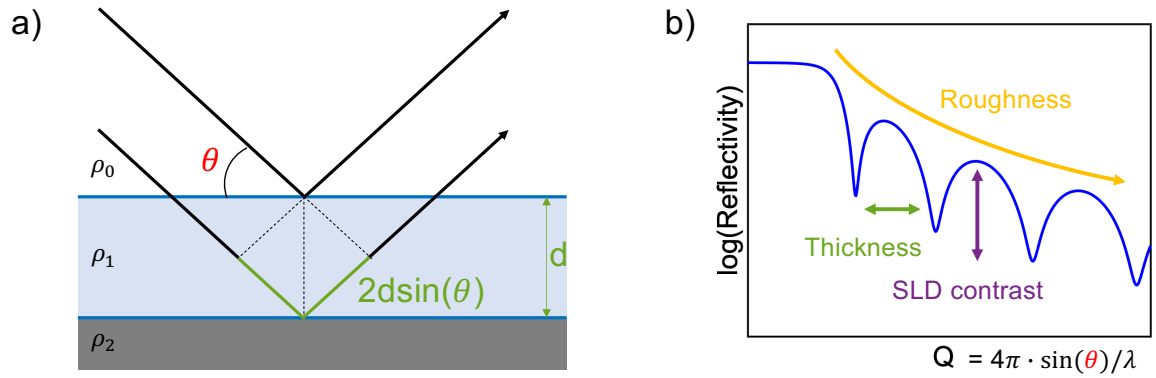

Figure 4.6. a) Two parts of a beam, reflected at the interfaces on each side of a layer. The path length difference is marked in green. b) Characteristic reflectivity curve.

4.3.1. Modeling

The reflectivity curve cannot be directly inverted to infer how the SLD varies at the interface which was measured. In principle, samples with very different SLD-profiles can give rise to identical reflectivity curves, and therefore, information must be extracted from reflectivity curves by fitting a model to the data,[86] as illustrated in figure 4.7. Reflectivity data (figure 4.7a) is used to fit a model which typically represents the SLD-profile of a sample using a set of "slabs", each corresponding to a material with a certain SLD, thickness and interfacial roughnesses towards the neighboring layers (figure 4.7b). Depending on prior knowledge about the sample, a selection of the parameter in the model is varied to fit the reflectivity data. Consequently, appropriate model selection is key to obtaining meaningful and accurate information from a reflectivity experiment.

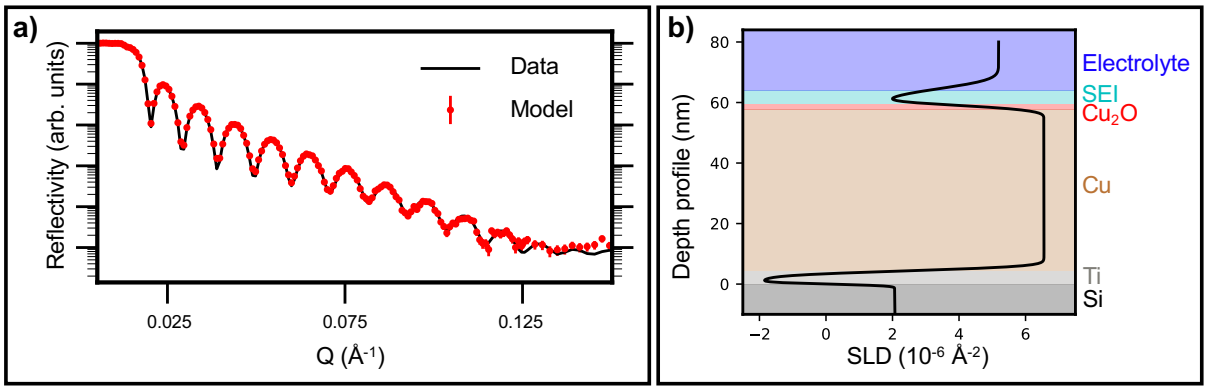

Figure 4.7. NR-data and the corresponding model. a) Reflectivity curve and the model which was fitted to this data. b) SLD profile of the model fitted in a), and materials assigned for each slab.

Chapter 5 - Results and Discussion

5.1. Highly concentrated electrolytes

The standard salt concentration around 1 mol/dm^3 frequently used for battery electrolytes typically maximizes the ionic conductivity of the electrolyte.[91] For a long time, the viscosity increase and resulting conductivity decrease for electrolytes with higher salt concentrations deterred researchers from investigating them more carefully, and only a few publications on the topic can be found before Yamada pioneered the field in the 2010s.[10,91–93] The reported benefits of highly concentrated electrolytes include improved rate capabilities in lithium-ion batteries, suppressed corrosion and extended the electrochemical stability window.[10,91] Moreover, HCEs have been shown to suppress dendrite growth on metal anodes and allow high-rate cycling with long cycle life and high Coulombic efficiencies.[11,94,95] Still, the mechanism(s) through which the highly concentrated electrolytes improve the performance of metal anodes is not well understood. Below, in our work, we have tried to address this.

5.1.1. Solvation structure

The solvation structure of liquid electrolytes can be probed using Raman spectroscopy, as an example, in figure 5.1a the Raman bands associated with CH_2 rocking and COC-stretching of the solvent 1,2-Dimethoxyethane (DME) are shown. When the salt potassium bis(fluorosulfonyl)imide (KFSI) is added to this solvent, spectral components at larger wavenumbers start to appear, which correspond to DME-molecules that are participating in the solvation of cations from the salt. By comparing the areas of the peaks related to free and solvating DME, the fraction of free solvent molecules in the electrolyte can be estimated (figure 5.1b).[96,97] In a 1 mol/kg electrolyte, roughly 10% of the DME molecules participate in the solvation of cations, whereas the corresponding number is 60% in a 4.34 mol/kg electrolyte (corresponding to a molar ratio of 1:2.5). Other DME-based electrolytes show similar behaviors. For NaTFSI/DME at the same molar ratio (1:2.5) as the 4.34 mol/kg KFSI/DME electrolyte, 68% of the DME molecules participate in the solvation.[96] Similarly, LiFSI/DME at the slightly more concentrated molar ratio 1:1.9 has been reported to have no or very little free solvent molecules.[98] The limited fraction of free solvent molecules (those that are not participating in the solvation shell of any ion) is characteristic for HCEs.[91,99] This electrolyte property also carries an important role for metal anodes, which is underlined by the observation that when HCEs are diluted with a non-interacting solvent that maintains their solvation structure, several of their benefits are retained.[100,101] Among other things, the electrolyte's solvation structure can be linked to the SEI formation process as solvent molecules' reductive stability change when they participate in the solvation of different ions.[85]

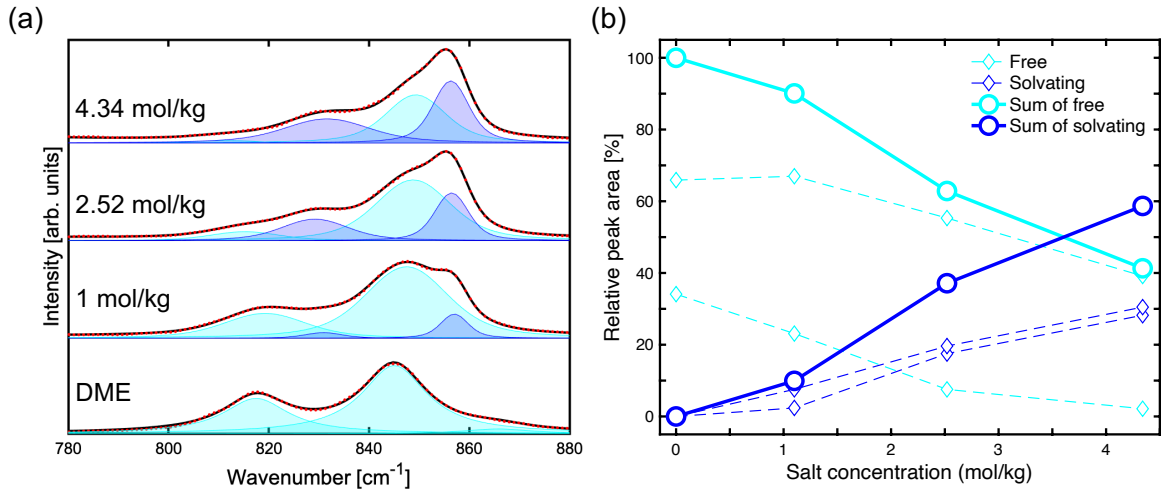

Figure 5.1. Solvation structures of KFSI/DME electrolytes with different salt concentrations. a) Raman spectra showing the CH_2-rocking and COC-stretching modes of DME. b) Relative peak areas for the peaks in a), indicating the fraction of solvating/free solvent molecules.

5.1.2. The SEI

The SEI-formation is often studied on a non-reacting substrate like Cu.[36] For alkali metal anodes, both electrochemical and chemical reactions will contribute to the SEI formation in a complex manner, while a non-reacting substrate provides a model system allowing a clearer separation of different processes. The different reactions contributing to the electrochemical SEI-formation can be probed using cyclic voltammetry. For a Cu electrode in a highly concentrated LiTFSI/DME electrolyte (figure 5.2a), a set of peaks are visible during the first anodic scan, corresponding to various electrolyte breakdown reactions. These reactions contribute to the formation of a passivating surface film, which is consistent with a significantly lower current observed in the anodic scan during the second cycle. Similarly, during the initial anodic scan on Cu in a highly concentrated KFSI/DME electrolyte, a broad peak around 0.8V and a sharper one at 0.1V appear (figure 5.2b). In the second cycle these peaks are absent or less pronounced. Apart from the different reference used to measure potentials, the differences between the CV curves in figure 5.2a and b can be attributed to the effect of electrolyte composition on the SEI-formation process. For instance, in the KFSI/DME electrolyte, metal deposition and SEI-formation reactions occur at potentials closer to each other than in the LiTFSI/DME system, evidenced by the peak at 0.1V during the anodic scan in figure 5.2b.

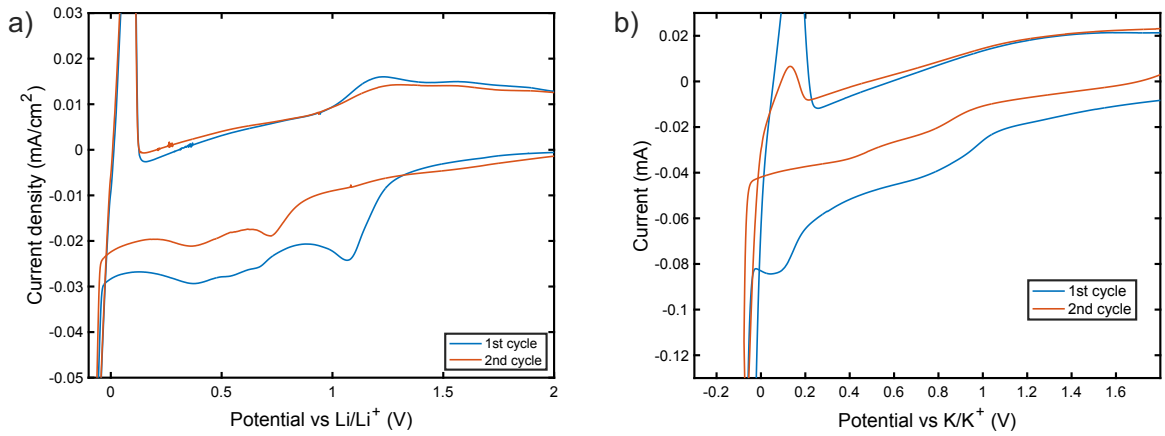

Figure 5.2. CV scans for Cu working electrodes in metal-Cu cells with a 1mV/s scan rate. a) Li-Cu two-electrode coin cell, using a highly concentrated LiTFSI/DME (1:2.2 molar ratio) electrolyte. b) K-Cu three electrode cell, using KFSI/DME (1:2.5 molar ratio).

Since the SEI forms from electrolyte breakdown reactions, we should expect that changing the electrolyte composition will affect the properties of the SEI layer. However, several other factors are also at play. To reiterate, the solvation structure will affect the reductive stability of solvent molecules.[85] Additionally, the concentration change of the reactants in themselves can have an effect and the shift of the equilibrium potential for metal deposition due to an increase of metal ions in the electrolyte can play a role.[91,102–104] Several reported benefits of HCEs can also be connected to their SEIs, like high rate capabilities in Li-ion batteries[10] and stabilization of Li-metal in highly concentrated LiTFSI/Acetonitrile solutions.[93]

Based on a couple of different arguments and observations, thin and compact SEIs have been suggested to form in HCEs. For instance, high CEs using HCEs have been used to argue that less SEI-growth takes place during cycling, resulting in a thin SEI. [91,94] The sputtering time necessary before metallic lithium can be detected on cycled lithium metal anodes using x-ray photoelectron spectroscopy has also been used to argue that thinner SEIs form in HCEs compared to electrolytes with lower salt concentrations.[105] However, there are several other mechanisms that can explain these phenomena, such as the formation of dead lithium. Instead, to support these observations and draw conclusions about SEI-layer thickness, we use *in situ* neutron reflectometry measurements to study Cu interfaces in LiTFSI/DME electrolytes with different LiTFSI concentrations. The reflectivity curves in figure 5.3a clearly change (compared to OCV) after a potentiostatic hold at 50 mV vs Li/Li$^+$ has been applied to form the SEI. To aid the interpretation of these changes, a slab model is created for the sample (figure 5.3b) and the layer thickness, SLD, as well as interfacial roughnesses, are fitted to account for the changes in the reflectivity. Our model explains differences between reflectivity curves at OCV and after the potentiostatic hold, through the formation of an SEI-layer with a low SLD (figure 5.3c). This is supported by the excellent agreement between model and experimental data (figure 5.3a). The fitted SEI-layer thickness is 13 nm for the LCE compared to 5 nm for the HCE, suggests that a HCE can aid the formation of a thin SEI-layer, in agreement with previous reports. TEM measurements have shown similar results for dilute and concentrated lithium

bis(pentafluoroethanesulfonyl)imide (LiBETI) in propylene carbonate solutions. The determined SEI layer thicknesses on lithium metal were 35 and 20 nm for electrolytes with 1.28 mol/kg or 3.27 mol/kg salt (molar ratios 1:7.7 and 1:3) after 30 cycles.[11]

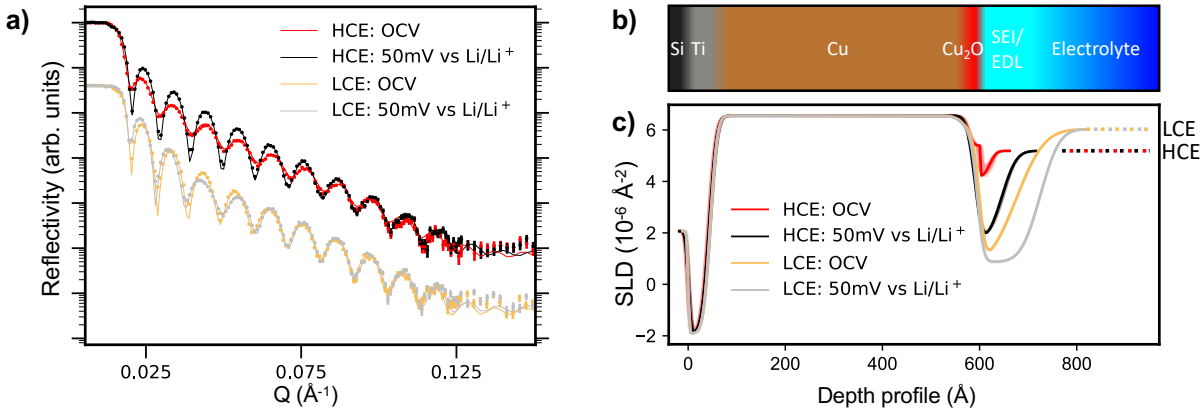

Figure 5.3. SEI-formation in LiTFSI/DME electrolytes with low (1:13.7 molar ratio, LCE) and high salt concentration (1:2.2 molar ratio, HCE). a) Reflectivity curves on a copper electrode in a Li-Cu cell before and after applying a potentiostatic hold to form the SEI. Markers represent the data and solid lines the fitted models. b) Schematic of the electrode surface models used to fit the data in a. c) SLD profile corresponding to the fitted models.

5.2. Plating and stripping

The impact of the electrode interface on the plating/stripping process can be illustrated by studying the voltage profiles of the K electrode in a K-Cu cell during galvanostatic cycling (figure 5.4). A large overpotential peak is observed at the onset of the first stripping from the K CE. This can be related to stripping from beneath a native oxide layer on the metal, which is associated with a large resistance. When “fresh” K is revealed, the stripping can proceed at a lower overpotential. In the second cycle, when K has been freshly deposited on the electrode, the stripping starts at a lower overpotential. Again, this can be linked to the lower interfacial resistance associated with stripping freshly deposited K. Once the deposits have been removed and K needs to be stripped from the bulk electrode, the overpotential increases. This gives rise to a step in the voltage profile of the CE (as well as the cell voltage). The appearance of these features in the voltage profile illustrate that the native oxide can drive non-uniform stripping.

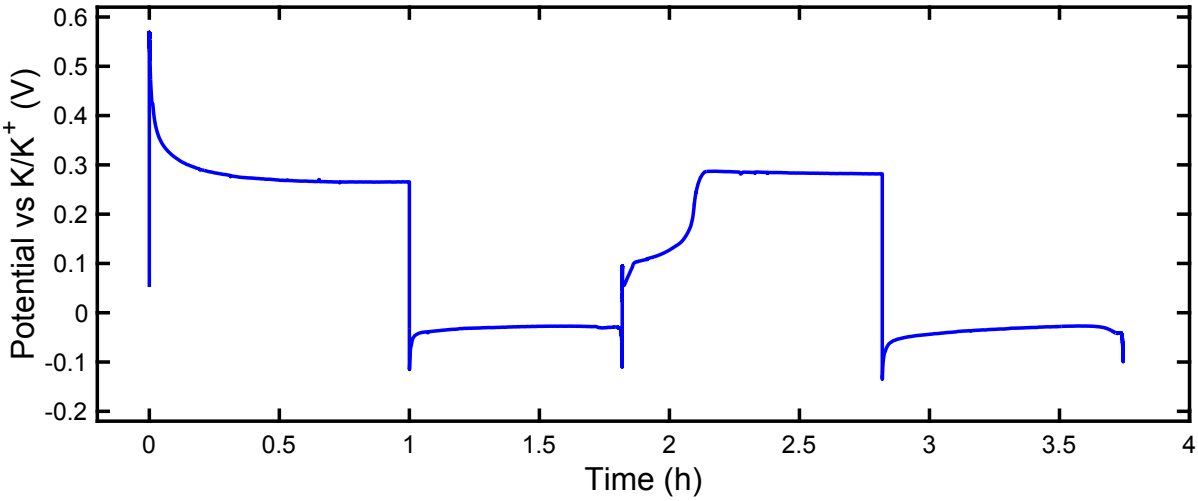

Figure 5.4. Electrode potential of the K electrode in a three-electrode K-Cu cell, cycled at 0.5 mA/cm^2 with a highly concentrated KFSI/DME electrolyte (1:2.5 molar ratio).

The deposition (stripping) on (from) a non-interacting substrate like Cu will also be affected by the SEI formation. At the onset of galvanostatic deposition on a non-interacting substrate, it is common to observe a peak in the voltage profile, which has been associated with the energy barrier for nucleation.[55] However, when K is deposited on a fresh Cu surface in a highly concentrated (1:2.5 molar ratio) KFSI/DME electrolyte (figure 5.5), this peak does not appear. On the other hand, the peak will appear if the SEI is formed already before the deposition, either through precycling or a potentiostatic hold. If the SEI is already formed, the K deposition (nucleation) will be the only faradic process that can produce significant amounts of current at the very beginning of the deposition. Since nucleation is associated with an energy barrier, a large overpotential is needed to drive the current until the deposition mechanism can transition to the growth of nuclei. On the other hand, during deposition on a fresh Cu surface, both SEI-formation and nucleation will happen simultaneously. Since this changes the rate at which nucleation occurs, and the overpotential needed for the nucleation to drive the nucleation is rate-dependent,[65] a nucleation peak no longer necessarily needs to appear. The nucleation peak is often used in the literature on metal anodes as a measure of the energy barrier for nucleation on a substrate,[55,56,65,106] which our results highlight is only accurate if there are no competing faradic processes.

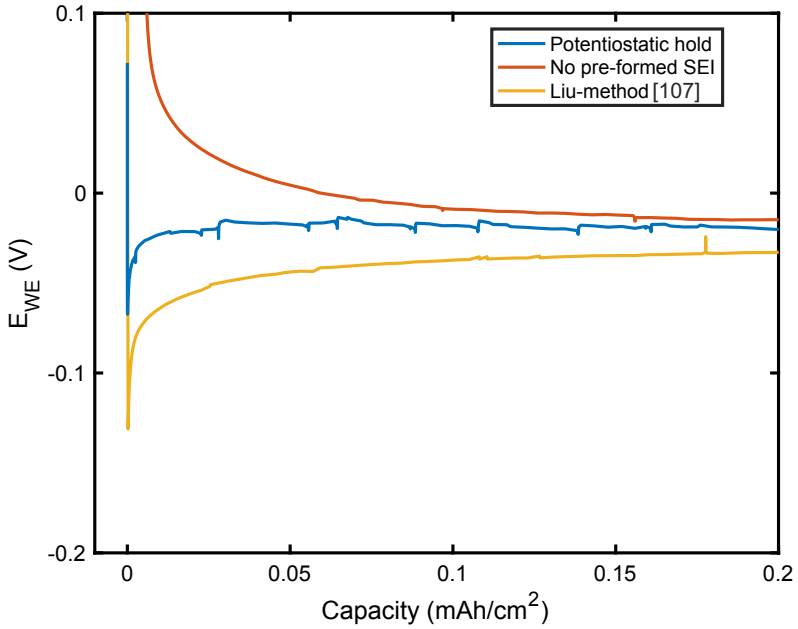

Figure 5.5. Galvanostatic deposition (0.5 mA/cm^2) in a K-Cu three-electrode cell after different SEI-formation steps: no formation-step, a potentiostatic hold at 50 mV vs K/K$^+$ and after a pre-cycling scheme described in [107]. Potentials are measured versus a K reference electrode, and the electrolyte is a highly concentrated KFSI/DME (1:2.5 molar ratio) electrolyte.

Chapter 6 - Conclusions and Outlook

Alkali metal stripping and plating processes are complex and can be affected by a wide range of different parameters and conditions. In this thesis, several connected issues are investigated. The electrolyte salt concentration changes the solvation structure, which will affect the SEI formation. In turn, the alkali metal plating and stripping can be connected to all these parameters. However, the results presented in this thesis point especially toward the importance of electrode interfaces and the SEI layer for controlling the stripping and deposition processes and solving the problems faced by metal anodes. This is illustrated, for instance, by the clear features in the voltage profiles of K-Cu cells, emanating from the different interfacial resistances at different parts of the electrode (paper 3). Clearly, characterizing and understanding the electrode interface is important, but the sensitivity of the SEI-layer makes experimental characterization challenging. In paper 2, we show that differences between SEI-layers formed in electrolytes with different compositions can be analyzed using *in situ* NR. However, the contrast in our experiment restricted us to quite simple models of the SEI while the measurement time was quite long (3h) and electrode areas rather large (≈25cm^2). To improve the utility of NR measurements for SEI layer characterization, it will be important to develop smaller measurement cells, more closely resembling standardized test cells like coin cells, enable faster measurements and find experiment designs with better contrast for the SEI layer. Developing better methods to characterize the SEI can also be a key to understanding why different electrolytes perform the way they do.

Additionally, a host of information about the stripping/plating processes can be gathered, simply by carefully analyzing the electrochemical data, as exemplified in paper 3. Still, by complementing the electrochemical data with *operando* characterization techniques, an even deeper understanding of the processes occurring at alkali metal anodes can be enabled. For instance, X-ray tomography can help to correlate electrochemical data with the electrode microstructures.[108]

Acknowledgments

First and foremost, I would like to thank my supervisor, Aleksandar Matic. Kindly enough, he let me come to his lab to learn a bit about what research is like 7 years ago. Since then, he has been patient and kind enough to let me stick around, while being so enthusiastic, selfless and fun to work with that I never regretted staying.

I would also like to thank my assistant supervisor Shizhao Xiong, thanks for being the best hypeman a young PhD can ask for, always dedicating time for my work and sharing your interest in metal anodes with me.

All the past and present group members of the Materials Physics division also deserve a big and warm collective thank you! Having been some kind of weird hang-around at the division for a lot of years, I have met so many great people who taught me a lot of interesting things and who made my time here truly enjoyable. I would like to especially thank Matthew Sadd for taking the time to answer my countless questions over the years, no matter how many brexit-jokes I made. Nataliia Mozhzhukhina also deserves a special thank you for being one of the best teachers a lost physicist could have in the black magic that is electrochemistry. Last but not least, next to no research would be done at the materials physics division if it wasn't for Ezio Zhangellini, thanks for all of your help over the years!

None of this work was done alone. Thank you to my excellent collaborators and co-authors! I would especially like to thank Anton Zubayer, who bravely took on the challenge of guiding a group of novices in the world of thin-film deposition and worked tirelessly to make our project a success. I would also like to thank Professor Jang-Yeon Hwang and his group for introducing me to the fascinating potassium-world.

Thanks to my friends and family for encouraging me and putting up with my endless talk about thesis-writing lately. I look forward to spending some more time with all of you again and recharging my batteries until it is time to write the next thesis.

Finally, I would like to thank FORMAS for the funding that made this work possible and Institute Laue-Langevin for providing the beamtime for our reflectometry experiments at the SuperADAM beamline.

Bibliography

[1] X. Yu, N.S. Sandhu, Z. Yang, M. Zheng, Suitability of energy sources for automotive application – A review, Appl Energy. 271 (2020) 115169. https://doi.org/10.1016/j.apenergy.2020.115169.

[2] M. Armand, P. Axmann, D. Bresser, M. Copley, K. Edström, C. Ekberg, D. Guyomard, B. Lestriez, P. Novák, M. Petranikova, W. Porcher, S. Trabesinger, M. Wohlfahrt-Mehrens, H. Zhang, Lithium-ion batteries – Current state of the art and anticipated developments, J Power Sources. 479 (2020). https://doi.org/10.1016/j.jpowsour.2020.228708.

[3] J. Zheng, M.S. Kim, Z. Tu, S. Choudhury, T. Tang, L.A. Archer, Regulating electrodeposition morphology of lithium: Towards commercially relevant secondary Li metal batteries, Chem Soc Rev. 49 (2020) 2701–2750. https://doi.org/10.1039/c9cs00883g.

[4] W. Li, H. Wang, E. Matios, J. Luo, Combining theories and experiments to understand the sodium nucleation behavior towards safe sodium metal batteries, Chem Soc Rev. 49 (2020) 3783–3805. https://doi.org/10.1039/d0cs00033g.

[5] W. Zhang, J. Yin, W. Wang, Z. Bayhan, H.N. Alshareef, Status of rechargeable potassium batteries, Nano Energy. 83 (2021) 105792. https://doi.org/10.1016/j.nanoen.2021.105792.

[6] B. Lee, E. Paek, D. Mitlin, S.W. Lee, Sodium Metal Anodes: Emerging Solutions to Dendrite Growth, Chem Rev. (2019). https://doi.org/10.1021/acs.chemrev.8b00642.

[7] P. Liu, D. Mitlin, Emerging Potassium Metal Anodes: Perspectives on Control of the Electrochemical Interfaces, Acc Chem Res. 53 (2020) 1161–1175. https://doi.org/10.1021/acs.accounts.0c00099.

[8] M.D. Tikekar, S. Choudhury, Z. Tu, L.A. Archer, Design principles for electrolytes and interfaces for stable lithium-metal batteries, Nat Energy. 1 (2016) 1–7. https://doi.org/10.1038/nenergy.2016.114.

[9] J.G. Zhang, W. Xu, J. Xiao, X. Cao, J. Liu, Lithium Metal Anodes with Nonaqueous Electrolytes, Chem Rev. 120 (2020) 13312–13348. https://doi.org/10.1021/acs.chemrev.0c00275.

[10] Y. Yamada, J. Wang, S. Ko, E. Watanabe, A. Yamada, Advances and issues in developing salt-concentrated battery electrolytes, Nat Energy. 4 (2019) 269–280. https://doi.org/10.1038/s41560-019-0336-z.

[11] S.K. Jeong, H.Y. Seo, D.H. Kim, H.K. Han, J.G. Kim, Y.B. Lee, Y. Iriyama, T. Abe, Z. Ogumi, Suppression of dendritic lithium formation by using concentrated electrolyte solutions, Electrochem Commun. 10 (2008) 635–638. https://doi.org/10.1016/j.elecom.2008.02.006.

[12] E. Peled, The Electrochemical Behavior of Alkali and Alkaline Earth Metals in Nonaqueous Battery Systems—The Solid Electrolyte Interphase Model, J Electrochem Soc. 126 (1979) 2047–2051. https://doi.org/10.1149/1.2128859.

[13] G. Bieker, M. Winter, P. Bieker, Electrochemical in situ investigations of SEI and dendrite formation on the lithium metal anode, Physical Chemistry Chemical Physics. 17 (2015) 8670–8679. https://doi.org/10.1039/c4cp05865h.

[14] K.N. Wood, M. Noked, N.P. Dasgupta, Lithium metal anodes: Toward an improved understanding of coupled morphological, electrochemical, and mechanical behavior, ACS Energy Lett. 2 (2017) 664–672. https://doi.org/10.1021/acsenergylett.6b00650.

[15] W. Liu, P. Liu, D. Mitlin, Review of Emerging Concepts in SEI Analysis and Artificial SEI Membranes for Lithium, Sodium, and Potassium Metal Battery Anodes, Adv Energy Mater. (2020). https://doi.org/10.1002/aenm.202002297.

[16] D. Li, H. Hu, B. Chen, W.Y. Lai, Advanced Current Collector Materials for High-Performance Lithium Metal Anodes, Small. 18 (2022). https://doi.org/10.1002/smll.202200010.

[17] K. Schmidt-Rohr, How Batteries Store and Release Energy: Explaining Basic Electrochemistry, J Chem Educ. 95 (2018) 1801–1810. https://doi.org/10.1021/acs.jchemed.8b00479.

[18] K.W. Beard, T.B. Reddy, eds., Linden's Handbook of Batteries, 5th ed., McGraw-Hill, 2019.

[19] B. Scrosati, K.M. Abraham, W. Van Schalkwijk, J. Hassoun, eds., Lithium Batteries, John Wiley and Sons Inc, Hoboken, New Jersey, 2013.

[20] J.-M. Tarascon, M. Armand, Issues and challenges facing rechargeable lithium batteries, Nature. 414 (2001) 359–367. http://www.ncbi.nlm.nih.gov/pubmed/11713543.

[21] Y. Kato, Z. Ogumi, J.M.P. Martin, eds., Lithium-Ion Batteries, Pan Stanford Publishing, 2019.

[22] D. Billaud, E. McRae, A. Hérold, Synthesis and electrical resistivity of lithium-pyrographite intercalation compounds (stages I, II and III), Mater Res Bull. 14 (1979) 857–864. https://doi.org/10.1016/0025-5408(79)90149-1.

[23] R. Fong, U. von Sacken, J.R. Dahn, Studies of Lithium Intercalation into Carbons Using Nonaqueous Electrochemical Cells, J Electrochem Soc. 137 (1990) 2009–2013. https://doi.org/10.1149/1.2086855.

[24] M.S. Whittingham, Fanwood, N.J., Chalcogenide battery, 1977. https://patents.google.com/patent/US4009052A/en.

[25] M.S. Whittingham, Electrical Energy Storage and Intercalation Chemistry, Science (1979). 192 (1976) 1126–1127.

[26] X.B. Cheng, R. Zhang, C.Z. Zhao, Q. Zhang, Toward Safe Lithium Metal Anode in Rechargeable Batteries: A Review, Chem Rev. 117 (2017) 10403–10473. https://doi.org/10.1021/acs.chemrev.7b00115.

[27] U.S. Geological Survey, Mineral Commodity Summaries 2022, 2022.

[28] IEA, Net Zero by 2050, Paris, 2021.

[29] IEA, The Role of Critical Minerals in Clean Energy Transitions, Paris, 2021.

[30] K. Kubota, M. Dahbi, T. Hosaka, S. Kumakura, S. Komaba, Towards K-Ion and Na-Ion Batteries as "Beyond Li-Ion," Chemical Record. 18 (2018) 459–479. https://doi.org/10.1002/tcr.201700057.

[31] W. Liu, P. Liu, D. Mitlin, Tutorial review on structure-dendrite growth relations in metal battery anode supports, Chem Soc Rev. 49 (2020) 7284–7300. https://doi.org/10.1039/d0cs00867b.

[32] P. Bonnick, J. Muldoon, The Dr Jekyll and Mr Hyde of lithium sulfur batteries, Energy Environ Sci. (2020). https://doi.org/10.1039/d0ee02797a.

[33] J. Ding, H. Zhang, W. Fan, C. Zhong, W. Hu, D. Mitlin, Review of Emerging Potassium–Sulfur Batteries, Advanced Materials. 32 (2020) 1–29. https://doi.org/10.1002/adma.201908007.

[34] L. Ma, Y. Lv, J. Wu, Y. Chen, Z. Jin, Recent Advances in Emerging Non-Lithium Metal – Sulfur Batteries : A Review, 2100770 (2021) 1–28. https://doi.org/10.1002/aenm.202100770.

[35] H. Wang, D. Yu, C. Kuang, L. Cheng, W. Li, X. Feng, Z. Zhang, X. Zhang, Y. Zhang, Alkali Metal Anodes for Rechargeable Batteries, Chem. 5 (2019) 313–338. https://doi.org/10.1016/j.chempr.2018.11.005.

[36] H. Wu, H. Jia, C. Wang, J.G. Zhang, W. Xu, Recent Progress in Understanding Solid Electrolyte Interphase on Lithium Metal Anodes, Adv Energy Mater. 11 (2021). https://doi.org/10.1002/aenm.202003092.

[37] F. Hao, A. Verma, P.P. Mukherjee, Mechanistic insight into dendrite-SEI interactions for lithium metal electrodes, J Mater Chem A Mater. 6 (2018) 19664–19671. https://doi.org/10.1039/c8ta07997h.

[38] E. Peled, D. Golodnitsky, G. Ardel, Advanced Model for Solid Electrolyte Interphase Electrodes in Liquid and Polymer Electrolytes, J Electrochem Soc. 144 (1997) L208–L210. https://doi.org/10.1149/1.1837858.

[39] S. Shi, P. Lu, Z. Liu, Y. Qi, L.G. Hector, H. Li, S.J. Harris, Direct calculation of Li-ion transport in the solid electrolyte interphase, J Am Chem Soc. 134 (2012) 15476–15487. https://doi.org/10.1021/ja305366r.

[40] Y. Zhou, M. Su, X. Yu, Y. Zhang, J.G. Wang, X. Ren, R. Cao, W. Xu, D.R. Baer, Y. Du, O. Borodin, Y. Wang, X.L. Wang, K. Xu, Z. Xu, C. Wang, Z. Zhu, Real-time mass spectrometric characterization of the solid–electrolyte interphase of a lithium-ion

battery, Nat Nanotechnol. 15 (2020) 224–230. https://doi.org/10.1038/s41565-019-0618-4.

[41] A. Zaban, D. Aurbach, Impedance spectroscopy of lithium and nickel electrodes in propylene carbonate solutions of different lithium salts A comparative study, J Power Sources. 54 (1995) 289–295. https://doi.org/10.1016/0378-7753(94)02086-I.

[42] Y. Ein-Eli, New perspective on the foundation and structure of the solid electrolyte interface at the graphite anode of Li-ion cells, Electrochemical and Solid-State Letters. 2 (1999) 212–214. https://doi.org/10.1149/1.1390787.

[43] Y. Li, Y. Li, A. Pei, K. Yan, Y. Sun, C.L. Wu, L.M. Joubert, R. Chin, A.L. Koh, Y. Yu, J. Perrino, B. Butz, S. Chu, Y. Cui, Atomic structure of sensitive battery materials and interfaces revealed by cryo–electron microscopy, Science (1979). 358 (2017) 506–510. https://doi.org/10.1126/science.aam6014.

[44] Z. Zhang, Y. Li, R. Xu, W. Zhou, Y. Li, S.T. Oyakhire, Y. Wu, J. Xu, H. Wang, Z. Yu, D.T. Boyle, W. Huang, Y. Ye, H. Chen, J. Wan, Z. Bao, W. Chiu, Y. Cui, Capturing the swelling of solid-electrolyte interphase in lithium metal batteries, Science (1979). 375 (2022) 66–70. https://doi.org/10.1126/science.abi8703.

[45] H. Liu, X.-B. Cheng, Z. Jin, R. Zhang, G. Wang, L.-Q. Chen, Q.-B. Liu, J.-Q. Huang, Q. Zhang, Recent advances in understanding dendrite growth on alkali metal anodes, EnergyChem. 1 (2019) 100003. https://doi.org/10.1016/j.enchem.2019.100003.

[46] C.J. Huang, B. Thirumalraj, H.C. Tao, K.N. Shitaw, H. Sutiono, T.T. Hagos, T.T. Beyene, L.M. Kuo, C.C. Wang, S.H. Wu, W.N. Su, B.J. Hwang, Decoupling the origins of irreversible coulombic efficiency in anode-free lithium metal batteries, Nat Commun. 12 (2021) 1–10. https://doi.org/10.1038/s41467-021-21683-6.

[47] X. Xu, X. Cheng, F. Jiang, S. Yang, D. Ren, P. Shi, H. Hsu, H. Yuan, J. Huang, M. Ouyang, Q. Zhang, Dendrite-accelerated thermal runaway mechanisms of lithium metal pouch batteries, SusMat. 2 (2022) 435–444. https://doi.org/10.1002/sus2.74.

[48] K.H. Chen, K.N. Wood, E. Kazyak, W.S. Lepage, A.L. Davis, A.J. Sanchez, N.P. Dasgupta, Dead lithium: Mass transport effects on voltage, capacity, and failure of lithium metal anodes, J Mater Chem A Mater. 5 (2017) 11671–11681. https://doi.org/10.1039/c7ta00371d.

[49] D. Aurbach, E. Zinigrad, Y. Cohen, H. Teller, A short review of failure mechanisms of lithium metal and lithiated graphite anodes in liquid electrolyte solutions, Solid State Ion. (2002) 405–416.

[50] G.M. Hobold, J. Lopez, R. Guo, N. Minafra, A. Banerjee, Y. Shirley Meng, Y. Shao-Horn, B.M. Gallant, Moving beyond 99.9% Coulombic efficiency for lithium anodes in liquid electrolytes, Nat Energy. 6 (2021) 951–960. https://doi.org/10.1038/s41560-021-00910-w.

[51] Z.W. Seh, J. Sun, Y. Sun, Y. Cui, A highly reversible room-temperature sodium metal anode, ACS Cent Sci. 1 (2015) 449–455. https://doi.org/10.1021/acscentsci.5b00328.

[52] S. Liu, J. Mao, Q. Zhang, Z. Wang, W.K. Pang, L. Zhang, A. Du, V. Sencadas, W. Zhang, Z. Guo, An Intrinsically Non-flammable Electrolyte for High-Performance Potassium Batteries, Angewandte Chemie International Edition. 59 (2020) 3638–3644. https://doi.org/10.1002/anie.201913174.

[53] E.M. Stuve, Overpotentials in Electrochemical Cells, in: Encyclopedia of Applied Electrochemistry, Springer New York, 2014: pp. 1445–1453. https://doi.org/10.1007/978-1-4419-6996-5.

[54] A.J. Bard, L.R. Faulkner, Electrochemical Methods: Fundamentals and Applications, 2nd ed., John Wiley & Sons, New York, 2000.

[55] P. Biswal, S. Stalin, A. Kludze, S. Choudhury, L.A. Archer, Nucleation and Early Stage Growth of Li Electrodeposits, Nano Lett. 19 (2019) 8191–8200. https://doi.org/10.1021/acs.nanolett.9b03548.

[56] P. Biswal, A. Kludze, J. Rodrigues, Y. Deng, T. Moon, S. Stalin, Q. Zhao, J. Yin, L.F. Kourkoutis, L.A. Archer, The early-stage growth and reversibility of Li electrodeposition in Br-rich electrolytes, Proc Natl Acad Sci U S A. 118 (2021) 1–11. https://doi.org/10.1073/pnas.2012071118.

[57] Y. Liu, X. Xu, M. Sadd, O.O. Kapitanova, V.A. Krivchenko, J. Ban, J. Wang, X. Jiao, Z. Song, J. Song, S. Xiong, A. Matic, Insight into the Critical Role of Exchange Current Density on Electrodeposition Behavior of Lithium Metal, Advanced Science. 8 (2021). https://doi.org/10.1002/advs.202003301.

[58] X. Xu, Y. Liu, J.-Y. Hwang, O.O. Kapitanova, Z. Song, Y.-K. Sun, A. Matic, S. Xiong, Role of Li-Ion Depletion on Electrode Surface: Underlying Mechanism for Electrodeposition Behavior of Lithium Metal Anode, Adv Energy Mater. n/a (n.d.) 2002390. https://doi.org/10.1002/aenm.202002390.

[59] V. Fleury, J.N. Chazalviel, M. Rosso, Coupling of drift, diffusion, and electroconvection, in the vicinity of growing electrodeposits, Phys Rev E. 48 (1993) 1279–1295. https://doi.org/10.1103/PhysRevE.48.1279.

[60] D. Rehnlund, C. Ihrfors, J. Maibach, L. Nyholm, Dendrite-free lithium electrode cycling via controlled nucleation in low LiPF6 concentration electrolytes, Materials Today. 21 (2018) 1010–1018. https://doi.org/10.1016/j.mattod.2018.08.003.

[61] H. Sano, H. Sakaebe, H. Senoh, H. Matsumoto, Effect of Current Density on Morphology of Lithium Electrodeposited in Ionic Liquid-Based Electrolytes, J Electrochem Soc. 161 (2014) A1236–A1240. https://doi.org/10.1149/2.0331409jes.

[62] Y. Liu, S. Xiong, J. Wang, X. Jiao, S. Li, C. Zhang, Z. Song, J. Song, Dendrite-free lithium metal anode enabled by separator engineering via uniform loading of lithiophilic nucleation sites, Energy Storage Mater. 19 (2019) 24–30. https://doi.org/10.1016/j.ensm.2018.10.015.

[63] R. Winand, Electrocrystallization- theory and applications, Hydrometallurgy. 29 (1992) 567–598.

[64] A. Milchev, Nucleation phenomena in electrochemical systems: thermodynamic concepts, ChemTexts. 2 (2016) 1–9. https://doi.org/10.1007/s40828-015-0022-0.

[65] A. Pei, G. Zheng, F. Shi, Y. Li, Y. Cui, Nanoscale Nucleation and Growth of Electrodeposited Lithium Metal, Nano Lett. 17 (2017) 1132–1139. https://doi.org/10.1021/acs.nanolett.6b04755.

[66] F. Shi, A. Pei, D.T. Boyle, J. Xie, X. Yu, X. Zhang, Y. Cui, Lithium metal stripping beneath the solid electrolyte interphase, Proc Natl Acad Sci U S A. 115 (2018) 8529–8534. https://doi.org/10.1073/pnas.1806878115.

[67] K.N. Wood, E. Kazyak, A.F. Chadwick, K.H. Chen, J.G. Zhang, K. Thornton, N.P. Dasgupta, Dendrites and pits: Untangling the complex behavior of lithium metal anodes through operando video microscopy, ACS Cent Sci. 2 (2016) 790–801. https://doi.org/10.1021/acscentsci.6b00260.

[68] X. Sun, X. Zhang, Q. Ma, X. Guan, W. Wang, J. Luo, Revisiting the Electroplating Process for Lithium-Metal Anodes for Lithium-Metal Batteries, Angewandte Chemie - International Edition. 59 (2020) 6665–6674. https://doi.org/10.1002/anie.201912217.

[69] W. Plieth, Electrochemistry for Materials Science, 1st ed., Elsevier, Amsterdam, 2008.

[70] O.B. Chae, J. Kim, B.L. Lucht, Modification of lithium electrodeposition behavior by variation of electrode distance, J Power Sources. 532 (2022) 231338. https://doi.org/10.1016/j.jpowsour.2022.231338.

[71] C. Brissot, M. Rosso, J.-N. Chazalviel, S. Lascaud, Dendritic growth mechanisms in lithiumrpolymer cells, J Power Sources. 81–82 (1999) 925–929.

[72] P. Bai, J. Li, F.R. Brushett, M.Z. Bazant, Transition of lithium growth mechanisms in liquid electrolytes, Energy Environ Sci. 9 (2016) 3221–3229. https://doi.org/10.1039/c6ee01674j.

[73] H.J.S. Sand, III. On the concentration at the electrodes in a solution, with special reference to the liberation of hydrogen by electrolysis of a mixture of copper sulphate and sulphuric acid , The London, Edinburgh, and Dublin Philosophical Magazine and Journal of Science. 1 (1901) 45–79. https://doi.org/10.1080/14786440109462590.

[74] J. Elezgaray, C. Léger, F. Argoul, Linear Stability Analysis of Unsteady Galvanostatic Electrodeposition in the Two-Dimensional Diffusion-Limited Regime, J Electrochem Soc. 145 (1998) 2016–2024. https://doi.org/10.1149/1.1838592.

[75] A. Mistry, C. Fear, R. Carter, C.T. Love, P.P. Mukherjee, Electrolyte Confinement Alters Lithium Electrodeposition, ACS Energy Lett. 4 (2019) 156–162. https://doi.org/10.1021/acsenergylett.8b02003.

[76] C. Monroe, J. Newman, The Impact of Elastic Deformation on Deposition Kinetics at Lithium/Polymer Interfaces, J Electrochem Soc. 152 (2005) A396. https://doi.org/10.1149/1.1850854.

[77] QuantumScape Corporation, Delivering on the promise of solid-state technology, (2022). https://www.quantumscape.com/technology/ (accessed October 20, 2022).

[78] Y. Liu, X. Xu, O.O. Kapitanova, P. v. Evdokimov, Z. Song, A. Matic, S. Xiong, Electro-Chemo-Mechanical Modeling of Artificial Solid Electrolyte Interphase to Enable Uniform Electrodeposition of Lithium Metal Anodes, Adv Energy Mater. 12 (2022). https://doi.org/10.1002/aenm.202103589.

[79] B.D. Adams, J. Zheng, X. Ren, W. Xu, J.G. Zhang, Accurate Determination of Coulombic Efficiency for Lithium Metal Anodes and Lithium Metal Batteries, Adv Energy Mater. 8 (2018). https://doi.org/10.1002/aenm.201702097.

[80] J. Xiao, Q. Li, Y. Bi, M. Cai, B. Dunn, T. Glossmann, J. Liu, T. Osaka, R. Sugiura, B. Wu, J. Yang, J.G. Zhang, M.S. Whittingham, Understanding and applying coulombic efficiency in lithium metal batteries, Nat Energy. 5 (2020) 561–568. https://doi.org/10.1038/s41560-020-0648-z.

[81] N. Elgrishi, K.J. Rountree, B.D. McCarthy, E.S. Rountree, T.T. Eisenhart, J.L. Dempsey, A Practical Beginner's Guide to Cyclic Voltammetry, J Chem Educ. 95 (2018) 197–206. https://doi.org/10.1021/acs.jchemed.7b00361.

[82] E.C. Cengiz, J. Rizell, M. Sadd, A. Matic, N. Mozhzhukhina, Review—Reference Electrodes in Li-Ion and Next Generation Batteries: Correct Potential Assessment, Applications and Practices, J Electrochem Soc. 168 (2021) 120539. https://doi.org/10.1149/1945-7111/ac429b.

[83] R. Nölle, K. Beltrop, F. Holtstiege, J. Kasnatscheew, T. Placke, M. Winter, A reality check and tutorial on electrochemical characterization of battery cell materials : How to choose the appropriate cell setup, Materials Today. 32 (2020) 131–146. https://doi.org/10.1016/j.mattod.2019.07.002.

[84] J.R. Ferraro, K. Nakamoto, C.W. Brown, Introductory Raman Spectroscopy, 2nd ed., Academic Press, 2003.

[85] X. Chen, H. Li, X. Shen, Q. Zhang, The Origin of the Reduced Reductive Stability of Ion–Solvent Complexes on Alkali and Alkaline Earth Metal Anodes, Angewandte Chemie. 130 (2018) 16885–16889. https://doi.org/10.1002/ange.201809203.

[86] J.A. Dura, E.D. Rus, P.A. Kienzle, B.B. Maranville, Nanolayer Analysis by Neutron Reflectometry, in: T. Imae (Ed.), Nanolayer Research, Elsevier B.V, 2017: pp. 155–202. https://doi.org/. http://dx.doi.org/10.1016/B978-0-444-63739-0.00005-0.

[87] J.E. Owejan, J.P. Owejan, S.C. Decaluwe, J.A. Dura, Solid electrolyte interphase in Li-ion batteries: Evolving structures measured in situ by neutron reflectometry, Chemistry of Materials. 24 (2012) 2133–2140. https://doi.org/10.1021/cm3006887.

[88] E.D. Rus, J.A. Dura, In Situ Neutron Reflectometry Study of Solid Electrolyte Interface (SEI) Formation on Tungsten Thin-Film Electrodes, ACS Appl Mater Interfaces. 11 (2019) 47553–47563. https://doi.org/10.1021/acsami.9b16592.

[89] R.K. Thomas, Neutron reflection from liquid interfaces, Annu Rev Phys Chem. 55 (2004) 391–426. https://doi.org/10.1146/annurev.physchem.54.011002.103830.

[90] F. Cousin, G. Fadda, An introduction to neutron reflectometry, EPJ Web Conf. 236 (2020) 04001. https://doi.org/10.1051/epjconf/202023604001.

[91] Y. Yamada, A. Yamada, Review—Superconcentrated Electrolytes for Lithium Batteries, J Electrochem Soc. 162 (2015) A2406–A2423. https://doi.org/10.1149/2.0041514jes.

[92] Y. Yamada, Y. Takazawa, K. Miyazaki, T. Abe, Electrochemical lithium intercalation into graphite in dimethyl sulfoxide-based electrolytes: Effect of solvation structure of lithium ion, Journal of Physical Chemistry C. 114 (2010) 11680–11685. https://doi.org/10.1021/jp1037427.

[93] Y. Yamada, K. Furukawa, K. Sodeyama, K. Kikuchi, M. Yaegashi, Y. Tateyama, A. Yamada, Unusual stability of acetonitrile-based superconcentrated electrolytes for fast-charging lithium-ion batteries, J Am Chem Soc. 136 (2014) 5039–5046. https://doi.org/10.1021/ja412807w.

[94] J. Qian, W.A. Henderson, W. Xu, P. Bhattacharya, M. Engelhard, O. Borodin, J.G. Zhang, High rate and stable cycling of lithium metal anode, Nat Commun. 6 (2015). https://doi.org/10.1038/ncomms7362.

[95] N. Xiao, W.D. Mcculloch, Y. Wu, Reversible Dendrite-Free Potassium Plating and Stripping Electrochemistry for Potassium Secondary Batteries, J. Am. Chem. Soc. 139 (2017) 2020. https://doi.org/10.1021/jacs.7b04945.

[96] R. Tatara, G.M. Leverick, S. Feng, S. Wan, S. Terada, K. Dokko, M. Watanabe, Y. Shao-Horn, Tuning NaO2 Cube Sizes by Controlling Na+ and Solvent Activity in Na-O2 Batteries, Journal of Physical Chemistry C. 122 (2018) 18316–18328. https://doi.org/10.1021/acs.jpcc.8b05418.

[97] T. Hosaka, T. Matsuyama, K. Kubota, R. Tatara, S. Komaba, KFSA/Glyme Electrolytes for 4V-Class K-Ion Batteries, J Mater Chem A Mater. 10 (2020) 23766–23771. https://doi.org/10.1039/d0ta08851j.

[98] Y. Yamada, M. Yaegashi, T. Abe, A. Yamada, A superconcentrated ether electrolyte for fast-charging Li-ion batteries, Chemical Communications. 49 (2013) 11194–11196. https://doi.org/10.1039/c3cc46665e.

[99] S.K. Jeong, M. Inaba, Y. Iriyama, T. Abe, Z. Ogumi, Electrochemical intercalation of lithium ion within graphite from propylene carbonate solutions, Electrochemical and Solid-State Letters. 6 (2003). https://doi.org/10.1149/1.1526781.

[100] K. Dokko, N. Tachikawa, K. Yamauchi, M. Tsuchiya, A. Yamazaki, E. Takashima, J.-W. Park, K. Ueno, S. Seki, N. Serizawa, M. Watanabe, Solvate Ionic Liquid Electrolyte for Li–S Batteries, J Electrochem Soc. 160 (2013) A1304–A1310. https://doi.org/10.1149/2.111308jes.

[101] X. Cao, H. Jia, W. Xu, J.-G. Zhang, Review—Localized High-Concentration Electrolytes for Lithium Batteries, J Electrochem Soc. 168 (2021) 010522. https://doi.org/10.1149/1945-7111/abd60e.

[102] H. Moon, T. Mandai, R. Tatara, K. Ueno, A. Yamazaki, K. Yoshida, S. Seki, K. Dokko, M. Watanabe, Solvent activity in electrolyte solutions controls electrochemical reactions in Li-Ion and Li-Sulfur batteries, Journal of Physical Chemistry C. 119 (2015) 3957–3970. https://doi.org/10.1021/jp5128578.

[103] H. Moon, R. Tatara, T. Mandai, K. Ueno, K. Yoshida, N. Tachikawa, T. Yasuda, K. Dokko, M. Watanabe, Mechanism of Li ion desolvation at the interface of graphite electrode and glyme-li salt solvate ionic liquids, Journal of Physical Chemistry C. 118 (2014) 20246–20256. https://doi.org/10.1021/jp506772f.

[104] K. Ueno, R. Tatara, S. Tsuzuki, S. Saito, H. Doi, K. Yoshida, T. Mandai, M. Matsugami, Y. Umebayashi, K. Dokko, M. Watanabe, Li+ solvation in glyme-Li salt solvate ionic liquids, Physical Chemistry Chemical Physics. 17 (2015) 8248–8257. https://doi.org/10.1039/c4cp05943c.

[105] L. Suo, Y.S. Hu, H. Li, M. Armand, L. Chen, A new class of Solvent-in-Salt electrolyte for high-energy rechargeable metallic lithium batteries, Nat Commun. 4 (2013). https://doi.org/10.1038/ncomms2513.

[106] K. Yan, Z. Lu, H.W. Lee, F. Xiong, P.C. Hsu, Y. Li, J. Zhao, S. Chu, Y. Cui, Selective deposition and stable encapsulation of lithium through heterogeneous seeded growth, Nat Energy. 1 (2016). https://doi.org/10.1038/NENERGY.2016.10.

[107] P. Liu, H. Hao, H. Celio, J. Cui, M. Ren, Y. Wang, H. Dong, A.R. Chowdhury, T. Hutter, F.A. Perras, J. Nanda, J. Watt, D. Mitlin, Multifunctional Separator Allows Stable Cycling of Potassium Metal Anodes and of Potassium Metal Batteries, Advanced Materials. 2105855 (2021) 1–16. https://doi.org/10.1002/adma.202105855.

[108] P. Pietsch, V. Wood, X-Ray Tomography for Lithium Ion Battery Research: A Practical Guide, Annu Rev Mater Res. 47 (2017) 451–479. https://doi.org/10.1146/annurev-matsci-070616-123957.